Hindawi
Advances in Astronomy
Volume 2017, Article ID 2626495, 18 pages
https://doi.org/10.1155/2017/2626495

Review Article

Modeling Kelvin–Helmholtz Instability in Soft X-Ray Solar Jets

Ivan Zhelyazkov,[1] Ramesh Chandra,[2] and Abhishek K. Srivastava[3]

[1]*Faculty of Physics, Sofia University, 1164 Sofia, Bulgaria*
[2]*Department of Physics, Kumaun University, Nainital 263001, India*
[3]*Department of Physics, Indian Institute of Technology, Banaras Hindu University, Varanasi 221005, India*

Correspondence should be addressed to Ivan Zhelyazkov; izh@phys.uni-sofia.bg

Received 8 August 2016; Revised 16 October 2016; Accepted 1 December 2016; Published 8 February 2017

Academic Editor: Valery Nakariakov

Development of Kelvin–Helmholtz (KH) instability in solar coronal jets can trigger the wave turbulence considered as one of the main mechanisms of coronal heating. In this review, we have investigated the propagation of normal MHD modes running on three X-ray jets modeling them as untwisted and slightly twisted moving cylindrical flux tubes. The basic physical parameters of the jets are temperatures in the range of 5.2–8.2 MK, particle number densities of the order of 10^9 cm^{-3}, and speeds of 385, 437, and 532 km s^{-1}, respectively. For small density contrast between the environment and a given jet, as well as at ambient coronal temperature of 2.0 MK and magnetic field around 7 G, we have obtained that the kink ($m = 1$) mode propagating on moving untwisted flux tubes can become unstable in the first and second jets at flow speeds of ≅348 and 429 km s^{-1}, respectively. The KH instability onset in the third jet requires a speed of ≅826 km s^{-1}, higher than the observed one. The same mode, propagating in weakly twisted flux tubes, becomes unstable at flow speeds of ≅361 km s^{-1} for the first and of 443 km s^{-1} for the second jet. Except the kink mode, the twisted moving flux tube supports the propagation of higher ($m > 1$) MHD modes that can become unstable at accessible jets' speeds.

1. Introduction

Jets are considered to be ubiquitous confined plasma ejecta in the solar atmosphere. They have been extensively observed in the solar atmosphere in various wavebands, such as Hα [1, 2], Ca II H [3–5], EUV [6], and soft X-ray [7] in order to understand their multitemperature characteristics. X-ray jets were discovered by the Soft X-Ray Telescope (SXT) on board *Yohkoh* [8], as transient X-ray energy release and enhancement with apparent collimated ballistic motions of the plasma associated with the flares in X-ray bright points, emerging flux regions, or active regions (for details, see Shibata et al. [7]). As it has been pointed out by Shimojo et al. [9], jets from X-ray bright points in active regions most likely appear at the western edge of preceding sunspots and exhibit a recurrent plasma propulsion in the solar atmosphere. These X-ray jets are confined plasma dynamics with typical morphological properties, for example, $(1–40) \times 10^4$ km length, and the width of 5×10^3–10^5 km. Such jets possess apparent velocities of 10–1000 km s^{-1} and lifetime of 100–16,000 s [9]. The electron densities of the X-ray jets are of the orders of $(0.7–4) \times 10^9$ cm^{-3}. Their temperatures lie in the range of 3–8 MK with an average temperature of 5.6 MK [10].

In terms of spatial location jets can be classified as polar jets [11] and active region jets [12]. A study of polar jet parameters based on *Hinode* XRT observations was carried out by Savcheva et al. [13] who showed that jets preferably occur inside the polar coronal holes. Culhane et al. [11] have found from *Hinode*'s Extreme-ultraviolet Imaging Spectrometer (EIS) 40″ slot observations of a polar coronal hole that jet temperature ranges from 0.4 to 5.0 MK. The jet velocities had typical values that are mostly less than the Sun's escape velocity (618 km s^{-1}); therefore, in consequence most of the jets fall back in the lower solar atmosphere after their triggering. Using the XTR on *Hinode*, Cirtain et al. [14] conclude that X-ray jets in polar coronal holes have two distinct velocities: one near the Alfvén speed (~800 km s^{-1}) and another near the sound speed (200 km s^{-1}). Moreover, they were the first to give an evidence for the propagation of Alfvén waves in solar X-ray jets. Kim et al. [15] presented

the morphological and kinematic characteristics of three small-scale X-ray/EUV jets simultaneously observed by the *Hinode* XRT and the *Transition Region and Coronal Explorer (TRACE)*. While observing the coronal jets, for two different wavelength bands, they obtain matching characteristics for their projected speed (90–310 km s^{-1}), lifetime (100–2000 s), and size (1.1–5 × 10^5 km). Chifor at al. [12] have reported 2007 January 15/16 observations of a recurring jet situated on the west side of NOAA active region 10938. A strong blue-shifted component and an indication of a weak red-shifted component at the base of the jet were observed around T_e = 1.6 MK in these jets. The upflow velocities were observed exceeding up to 150 km s^{-1}. These jets were seen over a range of temperatures between 0.25 and 2.5 MK, while their estimated electron densities lie above 10^{11} cm^{-3} for the high-velocity upflow components. Yang et al. [16] presented simultaneous observations of three recurring jets in EUV and soft X-ray (SXR), which occurred in an active region on 2007 June 5. On comparing their morphological and kinematic properties, the authors have found that EUV and SXR jets had similar onset locations, directions, size, and terminal velocities. The three observed jets were having maximum Doppler velocities ranging from 25 to 121 km s^{-1} in the Fe XII λ195 line and from 115 to 232 km s^{-1} in the He II λ256 line. Extensive multi-instrument observations obtained simultaneously with the SUMER spectrometer on board the *Solar and Heliospheric Observatory (SoHO)*, with EIS and XRT on board *Hinode*, and with the Extreme-ultraviolet imagers (EUVI) of the Sun–Earth Connection Coronal and Heliospheric Investigation (SECCHI) instrument suite on board the Ahead and Behind *STEREO* spacecrafts were performed by Madjarska [17]. The dynamic process of X-ray jet formation and evolution has been derived in great detail. In particular, for the first time there was found spectroscopically a temperature of 12 MK (Fe XXIII 263.76 Å) and density of 4 × 10^{10} cm^{-3} in the quiet Sun. The author has clearly identified two types of upflows in which the first one was the collimated upflow along the open magnetic fields, and the second was the formation of a plasma cloud from the expelled bright point small-scale loops. Chandrashekhar et al. [18] studied the dynamics of two jets seen in a polar coronal hole with a combination of EIS and XRT/*Hinode* data. They found no evidence of helical motions in these events but detected a significant shift of the jet position in a direction normal to the jet axis, with a drift velocity of about 27 and 7 km s^{-1}, respectively.

The launch of the *Solar Dynamics Observatory (SDO)* [19] with the Atmospheric Imaging Assembly (AIA) [20, 21] opens a new page in observing the solar jets. Moschou et al. [22] have reported high cadence observations of solar coronal jets observed in the extreme-ultraviolet (EUV) 304 Å using Atmospheric Imaging Assembly (AIA) instrument on board *SDO*. They registered, in fact, coronal hole jets, with speeds of 94 to 760 km s^{-1} and lifetimes of the order of several tens of minutes. A detailed description of the dynamical behavior of a jet in an on-disk coronal hole observed with AIA/*SDO* was presented by Chandrashekhar et al. [23]. Their study reveals new evidence of plasma flows prior to the jet's initiation along the small-scale loops at the base of the jet. The authors have also found further evidence that flows along the jet consisting of multiple, quasi-periodic small-scale plasma ejections. In addition, spectroscopic analysis estimates temperature as Log 5.89 ± 0.08 K and electron densities as Log 8.75 ± 0.05 cm^{-3} in the observed jet. Measured properties of the registered transverse wave have provided evidence that strong damping of the wave occurred as it propagates along the jet with speeds of ~110 km s^{-1}. Using the magnetoseismological inversion, observed plasma, and wave parameters, the jet's magnetic field is estimated as B = 1.21 ± 0.2 G. Recently, Sterling et al. [24] have reported high-resolution X-ray and extreme-ultraviolet observations of 20 randomly selected X-ray jets that form in coronal holes at the solar polar caps. In each jet, converse to the widely accepted emerging magnetic flux model, a miniature version of the filament eruptions that initiated coronal mass ejections drove the jet producing reconnection process. Formation of a rotating jet during the filament eruption on 2013 April 10–11 on the base of multiwavelength and multiviewpoint observations with *STEREO*/SECCHI/EUVI and *SDO*/AIA was reported by Filippov et al. [25]. The confined eruption of the filament within a null-point topology, which is also known as an Eiffel tower magnetic field configuration, forms a twisted jet after magnetic reconnection near the null point. The sign of the helicity in the jet is observed the same as that of the sign of the helicity in the filament. It is noteworthy that the untwisting motion of the reconnected magnetic field lines gives rise to the accelerating plasma along the jet.

It is well established that the magnetic reconnection at different heights in the solar atmosphere plays a key role in triggering jet-like events. The magnetic reconnection between open and closed fields (standard reconnection scenario) is one of the well-known processes of the jet's occurrence [15, 26]. The jets emerging by this kind of mechanism are known as *standard jets* [3, 7, 27, 28]. Some other observational and simulation studies showed that the reconnection at the magnetic null in a fan-spine magnetic topology can also trigger jet-like events [29–32]. Eruptions of small arches, filaments, and flux ropes from within this type of magnetic field configurations can be responsible for reconnection and jets' occurring. These types of jets are known as *blowout jets* [28, 33, 34]. Moore et al. [35] used the full-disk He II 304 Å movies from the Atmospheric Imaging Assembly on *SDO* to study the cool ($T \sim 10^5$ K) component of X-ray jets observed in polar coronal holes by XRT. The AIA 304 Å movies revealed that most polar X-ray jets spin as they erupt. The authors examined 54 X-ray jets that were found in polar coronal holes in XRT movies sporadically taken during the first year of continuous operation of AIA (2010 May through 2011 April). These 54 jets were big and bright enough in the XRT images to be categorized as a standard jet or as a blowout jet. From the X-ray movies, 19 of the 54 jets appeared like standard jets, 32 appeared as blowout jets, and three were ambiguous and were not falling in any category. Moore et al. [36] have studied 14 large-scale solar coronal jets observed in Sun's pole. In EUV movies from the *SDO*/AIA, each jet was very similar to most X-ray and EUV jets erupting in coronal holes. However, each was exceptional in that it went

higher than most of the standard coronal jets. They were detected in the outer corona beyond $2.2\,R_\odot$ in images as observed from the *Solar and Heliospheric Observatory/Large Angle Spectroscopic Coronagraph* (*LASCO*/C2 coronagraph [37]).

Schmieder et al. [38] proposed a new model between the standard and blowout models, where magnetic reconnection occurs in the bald patches around some twisted field lines, one of whose foot points is open. Pariat et al. [39] included the magnetic field inclination and photospheric field distribution and performed another 3D numerical MHD model for the two different types of jet events: standard and blowout jets. We note also that stereoscopic studies (multiple points of view) have been carried out by the EUVI/SECCHI imagers on board the twin *STEREO* spacecraft to estimate the expected speed, motion, and morphology of polar coronal jets [40]. To sum up, the flux emergence [41, 42] and flux cancellation [43, 44] are the two main triggering processes that are known to be responsible for jets' occurrence. In few observational and primarily numerical studies the wave-induced reconnection has also been suggested as a cause for the onset of jet-like events [42, 45–47].

We consider magnetically structured X-ray solar jets as moving cylindrical magnetic flux tubes that support the excitation/propagation of various kind of magnetohydrodynamic (MHD) oscillations and waves. While in static solar atmospheric plasma the propagating MHD modes are stable, the axial motion of the flux tubes engenders a velocity jump at the tube surface which can trigger a Kelvin–Helmholtz (KH) instability. The KH instability arises at the interface of two fluid layers that move with different speeds (see, e.g., Chandrasekhar [48])—then a strong velocity shear arises near the interface between these two fluids forming a vortex sheet. This vortex sheet becomes unstable to the spiral-like perturbations at small spatial scales [49]. In cylindrical geometry, when a magnetic flux tube is axially moving, such a vortex sheet is evolved near tube's boundary and it may become unstable against KH instability provided that the tube axial velocity exceeds a critical value [50]. Further on, in the nonlinear stage of KH instability, this vortex sheet causes the conversion of the directed flow energy into turbulent energy making an energy cascade at smaller spatial scales [51].

The KH instability studying in various solar jets over the past decade arose from the fact that KH vortices were observed in solar prominences [52–54], in Sweet–Parker current sheets [55], in a coronal streamer [56], and in coronal mass ejections [57–61]. All these observations stimulated the modeling of KH instability in moving twisted magnetic flux tubes in nonmagnetic environment [62], in magnetic tubes of partially ionized plasma [63], in spicules [64–66], in photospheric tubes [67], in high-temperature and cool surges [68, 69], in dark mottles [70], at the boundary of rising coronal mass ejections [60, 61, 71, 72], in rotating, tornado-like magnetized jets [49], and in a chromospheric jet (fast disappearance of rapid red-shifted and blue-shifted excursions alongside a larger scale Hα jet) [73]. A more extensive review on modeling the KH instability in solar atmosphere jets the reader can be seen in Zhelyazkov [74] and references therein.

The first modeling of KH instability in X-ray jets was carried out by Vasheghani Farahani et al. [75] who explored transverse wave propagation along the detected by Cirtain et al. [14] coronal hole soft X-ray jets. Vasheghani Farahani et al. analyzed analytically, in the limit of thin magnetic flux tube, the dispersion relation of the kink MHD mode and have obtained that this mode is unstable against the KH instability when the critical jet velocity is equal to $4.47v_{\mathrm{A}} = 3576\,\mathrm{km\,s^{-1}}$ ($v_{\mathrm{A}} = 800\,\mathrm{km\,s^{-1}}$ is the Alfvén speed inside the jet). Numerical solving of the same dispersion relation when considering the jet and its environment as cold magnetized plasmas, carried out by Zhelyazkov [76, 77], yielded a little bit lower critical flow speed for the instability onset; namely, $4.31v_{\mathrm{A}} = 3448\,\mathrm{km\,s^{-1}}$. The lowest critical jet speed of $4.025v_{\mathrm{A}} = 3220\,\mathrm{km\,s^{-1}}$ was derived by numerically solving the wave dispersion relation without any approximations, that is, treating both media as compressible plasmas. But even the latter critical jet speed is still too high for the KH instability to be detected/observed in coronal hole soft X-ray jets. The reason for obtaining such high critical speeds is the circumstance that Vasheghani Farahani et al. [75] assumed an electron number density of the order of $10^8\,\mathrm{cm^{-3}}$ and magnetic field strength of 10 G.

Here, we study the propagation of kink and higher MHD modes in standard active region soft X-ray jets, notably jets #8, #11, and #16 of Shimojo and Shibata's set of sixteen observed flares and jets [10], and have shown that with one order higher electron densities, $\sim 10^9\,\mathrm{cm^{-3}}$, and moderate magnetic field, ~7 G, MHD modes in high-speed jets, like these ones, can become unstable against the KH instability at accessible jets speeds, except for jet #16 which requires a higher flow velocity. In the next section we list the basic physical parameters of jet #11 and the topology of magnetic fields inside and outside the moving flux tube modeling jet and also derive the wave dispersion equation for both untwisted and twisted tubes. The physical parameters of other two jets (#8 and #16) will be provided *en route* in the next section. The numerical solving MHD wave dispersion relations and the discussion of the conditions under which the KH instability can develop in such moving structures are presented in Section 3. The last section summarizes the main results obtained in this article and outlooks our future studies of KH instability in more complex (rotating) solar atmosphere jets.

2. Geometry, Magnetic Field Topology, and MHD Wave Dispersion Relations

We consider the soft X-ray jet as a straight cylinder of radius a and density ρ_{i} embedded in a uniform field environment with density ρ_{e}. We study the propagation of MHD waves in two magnetic configurations, notably in untwisted and twisted flux tubes. For an untwisted tube magnetic fields in both media are homogeneous and directed along the z-axis of our cylindrical coordinate system (r, ϕ, z): $\mathbf{B}_{\mathrm{i}} = (0, 0, B_{\mathrm{i}})$ and $\mathbf{B}_{\mathrm{e}} = (0, 0, B_{\mathrm{e}})$, respectively (see Figure 1).

The magnetic field inside the twisted tube is helicoid, $\mathbf{B}_{\mathrm{i}} = (0, B_{\mathrm{i}\phi}(r), B_{\mathrm{iz}}(r))$, while outside the tube the magnetic field is

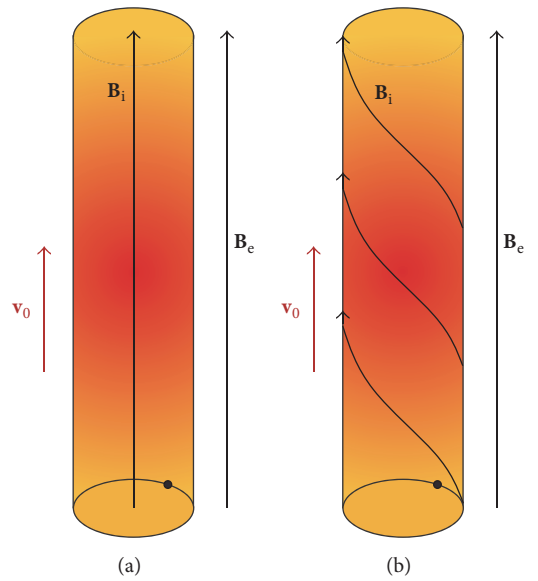

Figure 1: Equilibrium magnetic fields of a soft X-ray solar jet in an untwisted flux tube (a) and in a weakly twisted flux tube (b).

uniform and directed along the tube axis, $\mathbf{B}_e = (0, 0, B_e)$. Note that we assume a magnetic fields' equilibrium with uniform twist for which the magnetic field inside the tube is $\mathbf{B}_i = (0, Ar, B_{iz})$, where A and B_{iz} are constant. The parameter that characterizes the uniform magnetic field twist is the ratio $B_{i\phi}(a)/B_{iz} \equiv \varepsilon$, that is, $\varepsilon = Aa/B_{iz}$. Our frame of reference for studying the wave propagation in the jet is attached to the surrounding magnetoplasma—thus $\mathbf{v}_0 = (0, 0, v_0)$ represents the relative jet velocity, if there is any flow in the environment. The jump of the tangential velocity at the tube boundary then initiates the magnetic KH instability onset when the jump exceeds a critical value.

Before dealing with governing MHD equations, it is necessary to specify what kind of plasma each medium is (the moving tube and its environment). As seen from the Events List in [10], the electron density in jet #11 is $n_{jet} \equiv n_i = 2.9 \times 10^9\,\mathrm{cm}^{-3}$, the temperature is $T_{jet} \equiv T_i = 5.5$–$6.4\,\mathrm{MK}$, and jet speed (in their notation) is $V_{jet} = 437\,\mathrm{km\,s}^{-1}$. Our choice for environment magnetic field, electron density, and temperature is $B_e = 6.7\,\mathrm{G}$, $n_e = 2.6 \times 10^9\,\mathrm{cm}^{-3}$, and $T_e = 2.0\,\mathrm{MK}$, respectively. With $T_i = 5.5\,\mathrm{MK}$, the total pressure balance equation (equality of the sum of thermal and magnetic pressures in both media), that is,

$$p_i + \frac{B_i^2}{2\mu} = p_e + \frac{B_e^2}{2\mu}, \tag{1}$$

where μ is the magnetic permeability of vacuum, yields the following basic sound and Alfvén speeds in the jet and its environment: $c_{si} = 275\,\mathrm{km\,s}^{-1}$ and $v_{Ai} = 111\,\mathrm{km\,s}^{-1}$ and $c_{se} = 166\,\mathrm{km\,s}^{-1}$ and $v_{Ae} = 286\,\mathrm{km\,s}^{-1}$, respectively. Accordingly, the plasma betas in both media are $\beta_i = 7.369$ and $\beta_e = 0.403$—this implies that, in principle, one can treat the jet as incompressible plasma and its surrounding medium as cool magnetized plasma. When studying the MHD wave propagation in the untwisted magnetic flux tube we shall use two approaches, namely, of compressible plasmas in both media and the simplified limit of incompressible and cool plasmas—a similarity of dispersion curves patterns, obtained from corresponding dispersion relations, will eventually justify the usage of the second approach in particular in the case of twisted tube. There are two important input parameters in the modeling KH instability in moving magnetic flux tubes, which are the density contrast, $\rho_e/\rho_i \equiv \eta = 0.896$, and the ratio of the axial external and internal magnetic fields, $B_e/B_i \equiv b = 2.44$. For the twisted tube the second parameter has the form $b_{twist} = B_e/B_{iz}$.

In a system of cylindrical coordinates, the equilibrium physical variables (density, fluid velocity, and pressure) are functions of the radial coordinate r only. Then, their perturbations can be Fourier-analyzed putting them proportional to $\exp[\mathrm{i}(-\omega t + m\phi + k_z z)]$, where ω is the angular wave frequency (that, in general, can be a complex quantity), m is the mode number (a positive or negative integer), and k_z is the axial wave number. We can eliminate all except two of the perturbations (perturbation p_{tot} of the total (thermal + magnetic) pressure and the radial component ξ_r of the Lagrangian displacement $\boldsymbol{\xi}$) to get the following governing equations [78]:

$$D\frac{\mathrm{d}}{\mathrm{d}r}(r\xi_r) = C_1 r\xi_r - C_2 r p_{tot},$$
$$D\frac{\mathrm{d}p_{tot}}{\mathrm{d}r} = C_3\xi_r - C_1 p_{tot}. \tag{2}$$

The coefficients D, C_1, C_2, and C_3 are functions of the equilibrium variables ρ_0, $\mathbf{B}_0$, and $\mathbf{v}_0$ and of the Doppler-shifted frequency $\Omega = \omega - \mathbf{k}\cdot\mathbf{v}_0$ and have the following forms:

$$D = \rho_0\left(\Omega^2 - \omega_A^2\right)C_4,$$
$$C_1 = \frac{2B_{0\phi}}{\mu r}\left(\Omega^4 B_{0\phi} - \frac{m}{r}f_B C_4\right),$$

$$C_2 = \Omega^4 - \left(k_z^2 + \frac{m^2}{r^2}\right) C_4,$$

$$C_3 = \rho_0 D \left[\Omega^2 - \omega_A^2 + \frac{2B_{0\phi}}{\mu\rho_0}\frac{\mathrm{d}}{\mathrm{d}r}\left(\frac{B_{0\phi}}{r}\right)\right] + 4\Omega^4\left(\frac{B_{0\phi}^2}{\mu r}\right)^2 - \rho_0 C_4 \frac{4B_{0\phi}^2}{\mu r^2}\omega_A^2, \tag{3}$$

where

$$C_4 = \left(c_s^2 + c_A^2\right)\left(\Omega^2 - \omega_c^2\right),$$

$$f_B = \frac{m}{r}B_{0\phi} + \mathbf{k}\cdot\mathbf{B}_0,$$

$$\omega_A^2 = \frac{f_B^2}{\mu\rho_0}, \tag{4}$$

$$\omega_c^2 = \frac{c_s^2}{c_s^2 + c_A^2}\omega_A^2.$$

Here ω_A is the Alfvén frequency and ω_c is the cusp frequency; the other notation is standard.

Eliminating ξ_r from (2), one obtains the well-known second-order ordinary differential equation [79–81]

$$\frac{\mathrm{d}^2 p_{\mathrm{tot}}}{\mathrm{d}r^2} + \left[\frac{C_3}{rD}\frac{\mathrm{d}}{\mathrm{d}r}\left(\frac{rD}{C_3}\right)\right]\frac{\mathrm{d}p_{\mathrm{tot}}}{\mathrm{d}r} + \left[\frac{C_3}{rD}\frac{\mathrm{d}}{\mathrm{d}r}\left(\frac{rC_1}{C_3}\right) + \frac{1}{D^2}\left(C_2C_3 - C_1^2\right)\right] p_{\mathrm{tot}} = 0. \tag{5}$$

By means of the solutions to (5) in both media, one can find the corresponding expressions for ξ_r, and after merging these solutions, together with those for p_{tot}, through appropriate boundary conditions at the interface $r = a$, one can derive the dispersion relation of the normal modes propagating in the moving magnetic flux tube.

2.1. Dispersion Relation of MHD Modes in an Untwisted Flux Tube. In an untwisted magnetic flux tube, the coefficient $C_1 = 0$, while $C_3 = \rho_0 D(\Omega^2 - \omega_A^2)$—then (5) takes the form

$$\frac{\mathrm{d}^2 p_{\mathrm{tot}}}{\mathrm{d}r^2} + \frac{1}{r}\frac{\mathrm{d}p_{\mathrm{tot}}}{\mathrm{d}r} - \left(m_0^2 + \frac{m^2}{r^2}\right) p_{\mathrm{tot}} = 0, \tag{6}$$

where

$$m_0^2 = -\frac{\left(\Omega^2 - k_z^2 c_s^2\right)\left(\Omega^2 - k_z^2 v_A^2\right)}{\left(c_s^2 + v_A^2\right)\left(\Omega^2 - \omega_c^2\right)}. \tag{7}$$

The cusp frequency, ω_c, is usually expressed via the so-called tube speed, c_T, notably $\omega_c = k_z c_T$, where [82]

$$c_T = \frac{c_s v_A}{\sqrt{c_s^2 + v_A^2}}. \tag{8}$$

The solutions for p_{tot} can be written in terms of modified Bessel functions: $I_m(m_{0\mathrm{i}}r)$ inside the jet and $K_m(m_{0\mathrm{e}}r)$ in its surrounding plasma. We note that wave attenuation coefficients, $m_{0\mathrm{i}}$ and $m_{0\mathrm{e}}$, in both media are calculated from (7) with replacing the sound and Alfvén speeds with the corresponding values for each medium. Recall that, in evaluating $m_{0\mathrm{e}}$, the wave frequency is not Doppler-shifted—it is simply ω. By expressing the Lagrangian displacements ξ_{ir} and ξ_{er} in both media via the derivatives of corresponding Bessel functions and by applying the boundary conditions for continuity of the pressure perturbation p_{tot} and ξ_r across the interface, $r = a$, one obtains the dispersion relation of normal MHD modes propagating in a flowing compressible jet surrounded by a static compressible plasma [65, 83, 84]

$$\frac{\rho_{\mathrm{e}}}{\rho_{\mathrm{i}}}\left(\omega^2 - k_z^2 v_{\mathrm{Ae}}^2\right) m_{0\mathrm{i}}\frac{I_m'\left(m_{0\mathrm{i}}a\right)}{I_m\left(m_{0\mathrm{i}}a\right)} - \left[\left(\omega - \mathbf{k}\cdot\mathbf{v}_0\right)^2 - k_z^2 v_{\mathrm{Ai}}^2\right] m_{0\mathrm{e}}\frac{K_m'\left(m_{0\mathrm{e}}a\right)}{K_m\left(m_{0\mathrm{e}}a\right)} = 0. \tag{9}$$

Due to the flowing plasma, the wave frequency is Doppler-shifted inside the jet. We recall that for the kink mode ($m = 1$) one defines the so-called kink speed [82]

$$c_{\mathrm{k}} = \left(\frac{\rho_{\mathrm{i}} v_{\mathrm{Ai}}^2 + \rho_{\mathrm{e}} v_{\mathrm{Ae}}^2}{\rho_{\mathrm{i}} + \rho_{\mathrm{e}}}\right)^{1/2} = \left(\frac{1 + B_{\mathrm{e}}^2/B_{\mathrm{i}}^2}{1 + \rho_{\mathrm{e}}/\rho_{\mathrm{i}}}\right)^{1/2} v_{\mathrm{Ai}}, \tag{10}$$

which, as seen, is independent of sound speeds and characterizes the propagation of transverse perturbations. We will show that notably the kink mode can become unstable against KH instability.

When the jet is considered as incompressible plasma and its environment as a cool one, the MHD wave dispersion relation (9) keeps its form, but the two attenuation coefficients $m_{0\mathrm{i,e}}$ become much simpler, namely,

$$m_{0\mathrm{i}} = k_z,$$

$$m_{0\mathrm{e}} = \frac{\left(k_z^2 v_{\mathrm{Ae}}^2 - \omega^2\right)^{1/2}}{v_{\mathrm{Ae}}}, \tag{11}$$

respectively.

2.2. Dispersion Relation of MHD Normal Modes in a Twisted Flux Tube. Inside the tube ($r \leqslant a$), where $B_{\mathrm{i}\phi} = Ar$, the quantities f_B and ω_{Ai} take the forms

$$f_B = mA + k_z B_{\mathrm{iz}},$$

$$\omega_{\mathrm{Ai}} = \frac{mA + k_z B_{\mathrm{iz}}}{\sqrt{\mu\rho_{\mathrm{i}}}}, \tag{12}$$

respectively. For incompressible plasma, we redefine (without the loss of generality) the coefficients D, C_1, C_2, and C_3 by dividing them by C_4 to obtain

$$D = \rho\left(\Omega^2 - \omega_A^2\right),$$

$$C_1 = -\frac{2mB_\phi}{\mu r^2}\left(\frac{m}{r}B_\phi + k_z B_z\right),$$

$$C_2 = -\left(\frac{m^2}{r^2} + k_z^2\right), \tag{13}$$

$$C_3 = D^2 + D\frac{2B_\phi}{\mu}\frac{\mathrm{d}}{\mathrm{d}r}\left(\frac{B_\phi}{r}\right) - \frac{4B_\phi^2}{\mu r^2}\rho\omega_A^2.$$

Radial displacement ξ_r is expressed through the total pressure perturbation as

$$\xi_r = \frac{D}{C_3}\frac{\mathrm{d}p_{\mathrm{tot}}}{\mathrm{d}r} + \frac{C_1}{C_3}p_{\mathrm{tot}}. \tag{14}$$

The solution to this equation obviously depends upon the magnetic field and density profile.

With aforementioned coefficients D, C_1, C_2, and C_3, evaluated for the jet's medium, (5) reduces to the modified Bessel equation

$$\left[\frac{\mathrm{d}^2}{\mathrm{d}r^2} + \frac{1}{r}\frac{\mathrm{d}}{\mathrm{d}r} - \left(m_{0\mathrm{i}}^2 + \frac{m^2}{r^2}\right)\right] p_{\mathrm{tot}} = 0, \tag{15}$$

where

$$m_{0\mathrm{i}}^2 = k_z^2\left[1 - \frac{4A^2\omega_{\mathrm{Ai}}^2}{\mu\rho_{\mathrm{i}}\left(\Omega^2 - \omega_{\mathrm{Ai}}^2\right)^2}\right]. \tag{16}$$

The solution to (15) bounded at the tube axis is

$$p_{\mathrm{tot}}\left(r \leqslant a\right) = \alpha_{\mathrm{i}} I_m\left(m_{0\mathrm{i}} r\right), \tag{17}$$

where I_m is the modified Bessel function of order m and α_{i} is a constant. Lagrangian displacement ξ_{ir}, by using (14) can be written as

$$\xi_{ir} = \frac{\alpha_{\mathrm{i}}}{r}\left\{\frac{\left(\Omega^2 - \omega_{\mathrm{Ai}}^2\right) m_{0\mathrm{i}} r I_m'\left(m_{0\mathrm{i}} r\right)}{\rho_{\mathrm{i}}\left(\Omega^2 - \omega_{\mathrm{Ai}}^2\right)^2 - 4A^2\omega_{\mathrm{Ai}}^2/\mu} - \frac{2mA\omega_{\mathrm{Ai}} I_m\left(m_{0\mathrm{i}} r\right)/\sqrt{\mu\rho_{\mathrm{i}}}}{\rho_{\mathrm{i}}\left(\Omega^2 - \omega_{\mathrm{Ai}}^2\right)^2 - 4A^2\omega_{\mathrm{Ai}}^2/\mu}\right\}, \tag{18}$$

where the prime sign means a differentiation with respect the Bessel function argument.

For the cool environment with a straight-line magnetic field $B_{ez} = B_{\mathrm{e}}$ and homogeneous density ρ_{e}, the C_{1-3} and D coefficients take the form

$$\begin{aligned} D &= \rho\left(\omega^2 - \omega_{\mathrm{A}}^2\right), \\ C_1 &= 0, \\ C_2 &= -\left[\frac{m^2}{r^2} + k_z^2\left(1 - \frac{\omega^2}{\omega_{\mathrm{A}}^2}\right)\right], \\ C_3 &= D^2. \end{aligned} \tag{19}$$

The total pressure perturbation outside the tube obeys the same Bessel equation as (15), but $m_{0\mathrm{i}}^2$ is replaced by

$$m_{0\mathrm{e}}^2 = k_z^2\left(1 - \frac{\omega^2}{\omega_{\mathrm{Ae}}^2}\right), \tag{20}$$

which coincides with the attenuation coefficient in the cool environment of an untwisted flux tube. The solution bounded at infinity now is

$$p_{\mathrm{tot}}\left(r > a\right) = \alpha_{\mathrm{e}} K_m\left(m_{0\mathrm{e}} r\right), \tag{21}$$

where K_m is the modified Bessel function of order m and α_{e} is a constant.

In this case, the Lagrangian displacement can be written as

$$\xi_{\mathrm{er}} = \frac{\alpha_{\mathrm{e}}}{r}\frac{m_{0\mathrm{e}} r K_m'\left(m_{0\mathrm{e}} r\right)}{\rho_{\mathrm{e}}\left(\omega^2 - \omega_{\mathrm{Ae}}^2\right)}, \tag{22}$$

and the Alfvén frequency is simplified to

$$\omega_{\mathrm{Ae}} = \frac{k_z B_{ez}}{\sqrt{\mu\rho_{\mathrm{e}}}} = k_z v_{\mathrm{Ae}}. \tag{23}$$

Here, $v_{\mathrm{Ae}} = B_{\mathrm{e}}/\sqrt{\mu\rho_{\mathrm{e}}}$ is the Alfvén speed in the surrounding magnetized plasma.

The boundary conditions which merge the solutions of the Lagrangian displacement and total pressure perturbation inside and outside the twisted magnetic flux tube have the forms [85]

$$\begin{aligned} \xi_{\mathrm{ir}}\big|_{r=a} &= \xi_{\mathrm{er}}\big|_{r=a}, \\ p_{\mathrm{tot\,i}} - \frac{B_{\mathrm{i}\phi}^2}{\mu a}\xi_{ir}\bigg|_{r=a} &= p_{\mathrm{tot\,e}}\big|_{r=a}, \end{aligned} \tag{24}$$

where total pressure perturbations $p_{\mathrm{tot\,i}}$ and $p_{\mathrm{tot\,e}}$ are given by (17) and (21), respectively. With the help of these boundary conditions we derive the dispersion relation of the normal MHD modes propagating along a twisted magnetic flux tube with axial mass flow $\mathbf{v}_0$

$$\frac{\left(\Omega^2 - \omega_{\mathrm{Ai}}^2\right) F_m\left(m_{0\mathrm{i}} a\right) - 2mA\omega_{\mathrm{Ai}}/\sqrt{\mu\rho_{\mathrm{i}}}}{\left(\Omega^2 - \omega_{\mathrm{Ai}}^2\right)^2 - 4A^2\omega_{\mathrm{Ai}}^2/\mu\rho_{\mathrm{i}}} = \frac{P_m\left(m_{0\mathrm{e}} a\right)}{\left(\rho_{\mathrm{e}}/\rho_{\mathrm{i}}\right)\left(\omega^2 - \omega_{\mathrm{Ae}}^2\right) + A^2 P_m\left(m_{0\mathrm{e}} a\right)/\mu\rho_{\mathrm{i}}}, \tag{25}$$

where, as we already mentioned, $\Omega = \omega - \mathbf{k}\cdot\mathbf{v}_0$ is the Doppler-shifted wave frequency in the moving medium,

$$\begin{aligned} F_m\left(m_{0\mathrm{i}} a\right) &= \frac{m_{0\mathrm{i}} a I_m'\left(m_{0\mathrm{i}} a\right)}{I_m\left(m_{0\mathrm{i}} a\right)}, \\ P_m\left(m_{0\mathrm{e}} a\right) &= \frac{m_{0\mathrm{e}} a K_m'\left(m_{0\mathrm{e}} a\right)}{K_m\left(m_{0\mathrm{e}} a\right)}. \end{aligned} \tag{26}$$

This dispersion equation is similar to the dispersion equation of normal MHD modes in a twisted flux tube surrounded by incompressible plasma [65]—the only difference is that, there in (10), $\kappa_{\mathrm{e}} \equiv m_{0\mathrm{e}} = k_z$.

3. Numerical Solutions and Results

Firstly we shall study the dispersion characteristics of the kink ($m = 1$) mode in untwisted moving magnetic flux tube (in two approaches, notably (i) considering the jet and its surrounding plasma as compressible media and (ii) treating the jet as an incompressible medium while its environment is assumed to be cool plasma) and, later on, explore the same thing for the kink ($m = 1$) and higher ($m > 1$) MHD modes propagating in a twisted moving flux tube. Two

dispersion relations (9) and (25) are transcendent equations in which the wave frequency, ω, is a complex quantity: $\mathrm{Re}(\omega) + \mathrm{Im}(\omega)$, while the axial wave number, k_z, is a real variable. The appearance of KH instability (i.e., $\mathrm{Im}(\omega) > 0$) is determined primarily by the jet velocity and in searching for a critical/threshold value of it, we will gradually change velocity magnitude, v_0, from zero to that critical value (and beyond). Our numerical task is to solve the dispersion relation in complex variables, obtaining the real and imaginary parts of the wave frequency, or as is usually done, of the wave phase velocity $v_{\mathrm{ph}} = \omega/k_z$, as functions of the axial wave number, k_z, at various magnitudes of the velocity shear between the soft X-ray jet and its environment, $\mathbf{v}_0$.

For numerical solving the wave dispersion relations, it is practically to normalize all variables and we do that normalizing the wave length, $\lambda = 2\pi/k_z$, to the tube radius, a, that implies a dimensionless wave number $k_z a$. All speeds are normalized with respect to the Alfvén speed inside the jet, v_{Ai}. For normalizing the Alfvén speed in the ambient coronal plasma, v_{Ae}, we need the density contrast, η, and the ratio of the magnetic fields $b = B_{\mathrm{e}}/B_{\mathrm{i}}$, to find $v_{\mathrm{Ae}}/v_{\mathrm{Ai}} = b/\sqrt{\eta}$. The normalization of sound speeds in both media requires the specification of the reduced plasma betas, $\widetilde{\beta}_{\mathrm{i,e}} = c^2_{\mathrm{si,e}}/v^2_{\mathrm{Ai,e}}$. In the dimensionless computations, the flow speed, v_0, will be presented by the Alfvén Mach number $M_{\mathrm{A}} = v_0/v_{\mathrm{Ai}}$.

3.1. Kelvin–Helmholtz Instability in Untwisted Flux Tubes. Among the various MHD wave spectra that exist in a static magnetic field flux tube of compressible plasma, surrounded by compressible medium, the most interesting for us is the kink-speed wave whose speed for jet #11, according to (10), is equal to

$$c_{\mathrm{k}} = \sqrt{\frac{1+b^2}{1+\eta}}\, v_{\mathrm{Ai}} = 212.7\,\mathrm{km\,s^{-1}} \quad \text{or in dimensionless form } \frac{c_{\mathrm{k}}}{v_{\mathrm{Ai}}} = 1.9166. \tag{27}$$

The normal modes propagating in a static homogeneously magnetized flux tube can be pure surface waves, pseudo-surface (body) waves, or leaky waves (see Cally [86]). The type of the wave crucially depends on the ordering of the basic speeds in both media (the flux tube and its surrounding plasma), more specifically of sound and Alfvén speeds as well as corresponding tube speeds. In our case the ordering is

$$v_{\mathrm{Ai}} < c_{\mathrm{se}} < c_{\mathrm{si}} < v_{\mathrm{Ae}}, \tag{28}$$

which with $c_{\mathrm{Ti}} \cong 103\,\mathrm{km\,s^{-1}}$ and $c_{\mathrm{Te}} \cong 143.6\,\mathrm{km\,s^{-1}}$ after normalizing them with respect to the external sound speed, c_{se}, yields (in Cally's notation)

$$\begin{aligned} A &= 0.6687, \\ C &= 1.6566, \\ A_{\mathrm{e}} &= 1.7229, \\ C_{\mathrm{T}} &= 0.62, \\ C_{\mathrm{Te}} &= 0.8649. \end{aligned} \tag{29}$$

Since $A < C$ and $A < C_{\mathrm{Te}}$ along with $A < C_{\mathrm{Te}} < C$, according to Cally's classification, the kink mode in a rest flux tube must be pure surface mode type S^-_+ (for detail, see Cally [86]). For an S^-_+ type wave V should lie between A and C: $A \leqslant V \leqslant C$, and also $V < C_{\mathrm{Te}}$. In our normalization, the normalized wave velocity should be bracketed between 1 and $\sqrt{\widetilde{\beta}_{\mathrm{i}}} = 2.478$, that is, $1 \leqslant \omega/(k_z v_{\mathrm{Ai}}) \leqslant 2.478$. The typical wave dimensionless wave velocity $\omega/(k_z v_{\mathrm{Ai}})$ is the normalized kink speed $c_{\mathrm{k}}/v_{\mathrm{Ai}} = 1.9166$, which, as expected, lies between 1 and 2.478. Concerning the relation between normalized wave phase velocity and external tube speed, in our case we have the opposite inequality; that is, $V > C_{\mathrm{Te}}$, that in Cally's normalization reads as $1.2805 > 0.8649$ and in ours as $1.9166 > 1.2937$. The reason for that unexpected change in the mutual relations between two velocities is the relatively bigger value of parameter b (=2.44) that yields a larger magnitude of c_{k}, than, for example, in the case when b is close to 1—then the inequality $V < C_{\mathrm{Te}}$ is satisfied (see, e.g., Zhelyazkov et al. [87]).

A reasonable question is how the flow will change the dispersion characteristics of the kink ($m = 1$) mode. Calculations show that the flow shifts upwards the kink-speed dispersion curve and splits it into two separate curves [65]. (A similar duplication is observed for the tube-speed v_{Ti} dispersion curves, too.) The evolution of the pair of kink-speed dispersion curves can be seen in Figure 2(a)—the input parameters for solving the dispersion equation (9) of the kink mode ($m = 1$) traveling in a moving flux tube of compressible plasma surrounded by compressible coronal medium are $\eta = 0.896$, $b = 2.44$, $\widetilde{\beta}_{\mathrm{i}} = 6.141$, and $\widetilde{\beta}_{\mathrm{e}} = 0.336$. During calculations the Alfvén Mach number, M_{A}, was varied from zero (static plasma) to values at which we obtained unstable solutions. Let us first note that at $M_{\mathrm{A}} = 0$ we get the kink-speed dispersion curve which at a very small dimensionless wave number $k_z a$ (=0.005) yields the value of the normalized wave phase velocity equal to 1.9168—very close to the previously estimated magnitude of 1.9166. This observation implies that our code for solving the wave dispersion relation is correct. For small Alfvén Mach numbers the pair of kink-speed modes travel with velocities $M_{\mathrm{A}} \mp c_{\mathrm{k}}/v_{\mathrm{Ai}}$ [65] (in that case, their dispersion curves go practically parallel). At higher M_{A}, however, the behavior of each curve of the pair $M_{\mathrm{A}} \mp c_{\mathrm{k}}/v_{\mathrm{Ai}}$ turns out to be completely different. As seen from Figure 2(a), for $M_{\mathrm{A}} \geqslant 3.785$ both kink curves break and merge forming a family of semiclosed dispersion curves. A further increasing in M_{A} leads to a separation of those curves in opposite directions. This behavior of the kink ($m = 1$) mode dispersion curves signals us that we are in a range of the $\mathrm{Re}(v_{\mathrm{ph}}/v_{\mathrm{Ai}})$–$k_z a$-plane where one can expect the occurrence of KH instability. A prediction of the Alfvén Mach number M_{A} at which the instability will occur can be found from the inequality [88]

$$|m|\, M_{\mathrm{A}}^2 > \left(1 + \frac{1}{\eta}\right)\left(|m|\, b^2 + 1\right) \tag{30}$$

that gives for the kink ($m = 1$) mode $M_{\mathrm{A}} > 3.839$. In our case the KH instability starts at that M_{A}, for which the left-hand side semiclosed curve disappears—this happens at

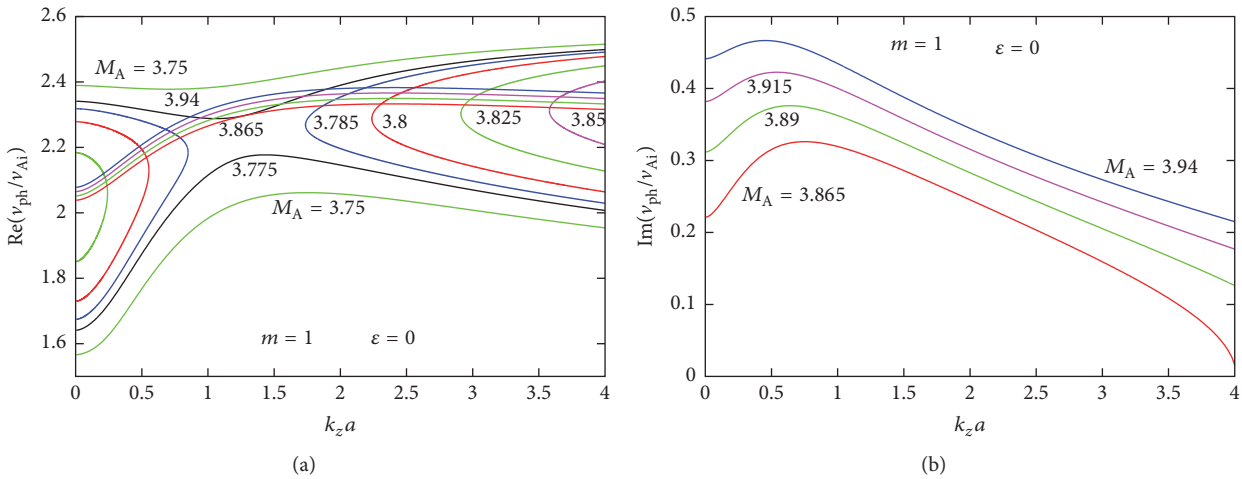

FIGURE 2: (a) Dispersion curves of stable and unstable kink ($m = 1$) MHD mode propagating in a moving untwisted magnetic flux tube of compressible plasma (modeling jet #11) at $\eta = 0.896$ and $b = 2.44$. Unstable dispersion curves located *above the middle of the plot* have been calculated for four values of the Alfvén Mach number $M_A = 3.865$, 3.89, 3.915, and 3.94. (b) The normalized growth rates of the unstable mode for the same values of M_A. Red curves in both plots correspond to the onset of KH instability.

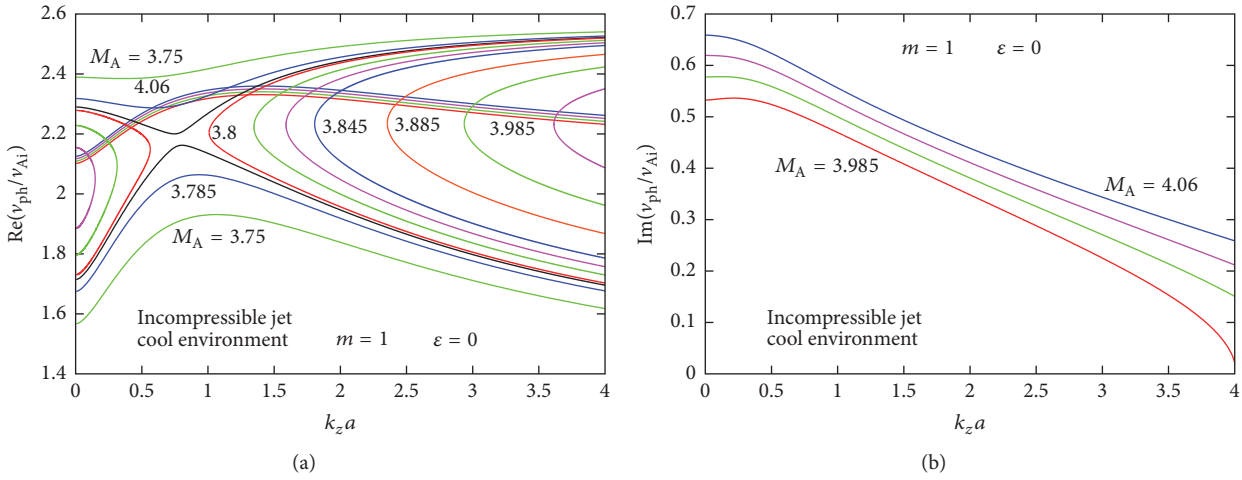

FIGURE 3: (a) Dispersion curves of stable and unstable kink ($m = 1$) MHD mode propagating in a moving untwisted magnetic flux tube of incompressible plasma surrounded by cool medium at the same input parameters as in Figure 2. The dispersion curves of unstable modes located *above the middle of the plot* have been calculated for $M_A = 3.985$, 4.01, 4.035, and 4.06. Alfvén Mach numbers associated with the nonlabeled black, green, and purple curves are equal to 3.796, 3.815, and 3.83, respectively, while those of far right green and purple semiclosed curves have magnitudes of 3.925 and 3.965. (b) Similar plots as in Figure 2.

$M_A^{cr} = 3.865$. The growth rates of unstable kink modes are plotted in Figure 2(b). The red curves in all diagrams denote the marginal dispersion/growth rate curves: for values of the Alfvén Mach number smaller than M_A^{cr} the kink mode is stable; otherwise it becomes unstable and the instability is of the KH type. With $M_A^{cr} = 3.865$ the kink mode will be unstable when the velocity of the moving flux tube is higher than 429 km s^{-1}—a speed, which is below than the observationally measured jet speed of 437 km s^{-1}. We would like to underline that all the stable kink modes in the untwisted ($\varepsilon = 0$) moving tube modeling jet #11 are pure surface modes while the unstable ones are not—the latter becomes partly surface and partly leaky modes (their external attenuation coefficients, m_{0e}s, are complex quantities with positive imaginary parts). This circumstance means that wave energy is radiated outward in the surrounding medium, which allows us to claim the KH instability plays a dual role: once in its nonlinear stage the instability can trigger wave turbulence and simultaneously the propagating KH-mode is radiating its energy outside.

When numerically solving (9) for the kink ($m = 1$) mode treating the jet's plasma as incompressible medium and its environment as cool plasma, we obtain dispersion curves' and growth rates' patterns very similar to those shown in Figure 2 (see Figure 3). Computations show, as expected, that the stable kink mode is a nonleaky surface mode, while the

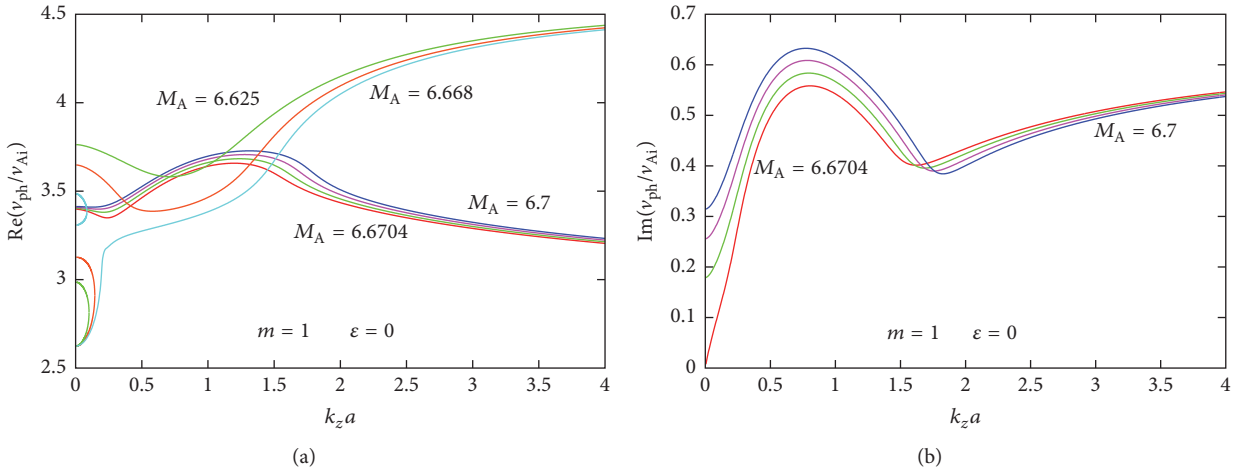

FIGURE 4: (a) Dispersion curves of stable and unstable kink ($m = 1$) MHD mode propagating in a moving untwisted magnetic flux tube of compressible plasma (modeling jet #8) at $\eta = 0.963$ and $b = 4.56$. Unstable mode's dispersion curves are pictured *in the middle of the plot* for $M_A = 6.6704$, 6.68, 6.69, and 6.7. (b) The corresponding normalized growth rates of unstable modes for the same values of M_A.

unstable one possesses a real internal attenuation coefficient, $m_{0i} = k_z$, not changed by the instability, but the external one, m_{0e}, becomes a complex quantity with positive real and negative imaginary parts. Now the threshold Alfvén Mach number is a little bit bigger and yields a critical jet speed for the instability onset of $\cong 442\,\mathrm{km\,s^{-1}}$, being with $5\,\mathrm{km\,s^{-1}}$ higher than the observationally measured $437\,\mathrm{km\,s^{-1}}$. We note that, as a rule, jet's incompressible plasma approximation yields slightly higher threshold Alfvén Mach numbers than the model of compressible media. This ascertainment shows how sensitive to jet's and its environment's media treatment the occurrence of KH instability of the kink mode in our jet is —one can expect instability onset at an accessible jet speed only if both media are considered as compressible magnetized plasmas.

The basic physical parameters of jet #8, namely $n_i = 4.1 \times 10^9\,\mathrm{cm^{-3}}$ and $T_i = 5.2\,\mathrm{MK}$, for a low density contrast of $\eta = 0.963$ assuming as before that the temperature of surrounding plasma is $T_e = 2.0\,\mathrm{MK}$ and the background magnetic field, B_e, is equal to 7 G, yield the following sound and Alfvén speeds: $c_{se} = 166\,\mathrm{km\,s^{-1}}$, $c_{si} = 267.5\,\mathrm{km\,s^{-1}}$, $v_{Ae} = 242.8\,\mathrm{km\,s^{-1}}$, and $v_{Ai} = 52.22\,\mathrm{km\,s^{-1}}$. Accordingly, plasma betas in both media are $\beta_i = 31.5$ and $\beta_e = 0.56$, while the magnetic fields ratio $b = 4.563$ defines $B_i = 1.53$ G. The speed ordering, $v_{Ai} < c_{se} < v_{Ae} < c_{si}$, according to Cally's [86] classification, tells us that in a rest magnetic flux tube the propagating wave must be a pure surface mode of type S_+^-. The numerical computations confirm this, as well as reproduce the normalized kink speed of 3.3342 within three places after the decimal point. With the flow inclusion, the behavior of the pair kink-speed dispersion curves in the region of the instability onset, as seen from Figure 4(a), is completely different; more specifically, the lower semiclosed kink-speed dispersion curves at $M_A = 6.625$ and 6.65 (the orange curve) correspond to pseudosurface (body) waves, while the higher kink-speed dispersion curves are associated with surface waves. Note that at $M_A = 6.668$ the surface wave dispersion curves brakes in two parts: the right-hand one merges with the lower kink-speed curve at $k_z a = 0.2337$ (see the blue line) while its left-hand side forms a narrow semiclosed dispersion curve of pure surface mode. The threshold Alfvén Mach number is equal to 6.6704 (the prediction one according to (30) is 6.67) which implies that the critical flow speed for KH instability onset is equal to $348.3\,\mathrm{km\,s^{-1}}$—a value far below the jet speed of $385\,\mathrm{km\,s^{-1}}$. This circumstance guarantees that even if one considers the jet medium as incompressible plasma and its environment as cool plasma we will get an accessible jet's speed for instability onset.

In a similar way, calculating the sound and Alfvén speeds for jet #16 and its environment (with $n_i = 1.0 \times 10^9\,\mathrm{cm^{-3}}$, $T_i = 7.4\,\mathrm{MK}$, $\eta = 0.95$, $T_e = 2.0\,\mathrm{MK}$, and $B_e = 6.7$ G) we get $c_{se} = 166\,\mathrm{km\,s^{-1}}$, $c_{si} \cong 319\,\mathrm{km\,s^{-1}}$, $v_{Ae} \cong 474\,\mathrm{km\,s^{-1}}$, $v_{Ai} = 350\,\mathrm{km\,s^{-1}}$, and plasma betas $\beta_i \cong 1.0$ and $\beta_e = 0.14$. The magnetic fields ratio, b, is equal to 1.32 giving $B_i \cong 5.1$ G. In this case, the speed ordering is $c_{se} < c_{si} < v_{Ai} < v_{Ae}$ and the kink ($m = 1$) mode propagating in a rest magnetic flux tube is a pseudosurface (body) wave of type B_+^- (see Table I in [86]). The numerical calculations confirm this mode type and yield a normalized value of the kink speed very close to the predicted one of 1.1858. Now the pattern of stable kink-speed dispersion curves is more complicated (see Figure 5(a))—while the regular lower kink-speed curves correspond to pseudosurface (body) waves, the higher kink-speed dispersion curves have the form of narrow and long semiclosed up to $M_A = 2.3$ loops and are in fact bulk waves: both attenuation coefficients are purely imaginary numbers. As expected, the dispersion curves of unstable kink mode possess complex attenuation coefficients (with positive real and imaginary parts for m_{0i} and positive real and negative imaginary part for m_{0e}). The threshold Alfvén Mach number being equal to 2.359305 determines a critical flow velocity of $825.8\,\mathrm{km\,s^{-1}}$ for KH instability onset which is much higher than the jet #16 speed of $532\,\mathrm{km\,s^{-1}}$. This consideration shows that even a relatively high-speed observed soft X-ray jet

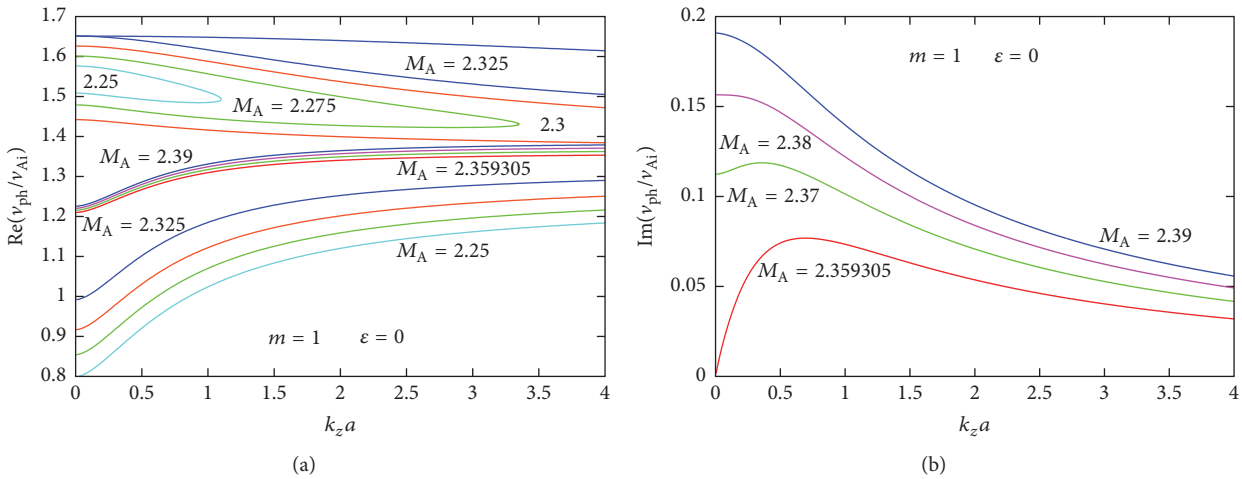

FIGURE 5: (a) Dispersion curves of stable and unstable kink ($m = 1$) MHD mode propagating in a moving untwisted magnetic flux tube of compressible plasma (modeling jet #16) at $\eta = 0.95$ and $b = 1.32$. Dispersion curves of unstable modes located *in the middle of the plot* have been calculated for $M_A = 2.359305$, 2.37, 2.38, and 2.39. (b) Plots of corresponding normalized growth rates.

cannot become unstable—the reason for that in this case is the low density of the jet's plasma.

3.2. Kelvin–Helmholtz Instability in Twisted Flux Tubes. A natural question that immediately raises is how the twist of the internal magnetic field, $\mathbf{B}_i$, will change the conditions for instability occurrence and the shape of the dispersion curves. When we model the soft X-ray jet as a moving twisted magnetic flux tubes, there are two types of instabilities that can develop in the jet: namely, kink instability due to the twist of the magnetic field and KH instability owing to the tangential discontinuity of plasma velocity at the tube boundary. According to Dungey and Loughhead [89], the kink instability will occur provided $B_{i\phi}(a) > 2B_{iz}$, or in our notation, as $\varepsilon > 2$. Further on, in order to prevent the developing of kink instability, we will consider weakly twisted flux tubes, $\varepsilon < 1$, and, thus, only KH instability can take place in such a jet configuration. When numerically solving dispersion equation (25) we need the normalization of the local Alfvén frequencies $\omega_{Ai,e}$. The normalization of these frequencies is performed by multiplying each of them by the tube radius, a, and dividing by the Alfvén speed $v_{Ai} = B_{iz}/\sqrt{\mu\rho_i}$ to get

$$\frac{a\omega_{Ai}}{v_{Ai}} = m\frac{Aa}{B_{iz}} + k_z a = m\varepsilon + k_z a,$$
$$\frac{a\omega_{Ae}}{v_{Ai}} = k_z a\frac{B_e/B_{iz}}{\sqrt{\eta}} = k_z a\frac{b_{twist}}{\sqrt{\eta}}, \quad (31)$$

where $b_{twist} = B_e/B_{iz} = b\sqrt{1+\varepsilon^2}$. For small values of ε, we will take $b_{twist} \cong b$.

We begin our calculations for the kink ($m = 1$) mode in the moving twisted tube (modeling jet #11) with $\eta = 0.896$, $b_{twist} \cong b = 2.44$, and $\varepsilon = 0.025$. The results of numerical task are presented in Figure 6, from which one sees that the kink mode dispersion and growth rate curves are very similar to those shown in Figure 3. The critical flow velocity for emerging KH instability now is $v_0^{cr} = 442.6\,\mathrm{km\,s^{-1}}$, calculated by using the "reduced" Alfvén speed $v_{Ai}/\sqrt{1+\varepsilon^2} = 110.96\,\mathrm{km\,s^{-1}}$. KH instability of the ($m = -1$) mode will occur if the jet speed exceeds $442\,\mathrm{km\,s^{-1}}$, of which value is beyond the observationally derived jet speed of $437\,\mathrm{km\,s^{-1}}$. We note that while the wave attenuation coefficient of the $m = 1$ mode propagating in untwisted moving magnetic flux tube of incompressible plasma surrounded by a cool medium is not changed by the flow, in the twisted flux tube (in the same approximations) that attenuation coefficient becomes a complex number with positive imaginary part, like the attenuation coefficient in the cool environment.

According to the instability criterion (30), the occurrence of KH instability of higher MHD modes would require lower threshold Alfvén Mach numbers (and accordingly lower critical jet speeds) than those of the kink ($m = \pm 1$) mode. Our computations show, however, that, with $\varepsilon = 0.025$, the threshold Alfvén Mach numbers are generally still high to initiate the KH instability. Their magnitudes for the $m = 2$, 3, and 4 modes are 3.965, 3.943, and 3.926, respectively. The corresponding critical velocities for instability onset are accordingly equal to 440.0, 437.5, and $435.6\,\mathrm{km\,s^{-1}}$. As seen, only the $m = 4$ MHD mode can become unstable against KH instability. A clutch of unstable dispersion curves and normalized growth rates are shown in Figure 7. Here we observe a new phenomenon: the KH instability starts at some critical $k_z a$-number along with the corresponding threshold Alfvén Mach number. That critical dimensionless wave number for the $m = 4$ MHD mode (look at Figure 7) is equal to 0.528. If we assume that jet #11 has a width $\Delta\ell = 5 \times 10^3$ km, then the critical wavelength for a KH instability emergence is $\lambda_{cr}^{m=4} \cong 29.8$ Mm.

A substantial decrease in the threshold Alfvén Mach number in moving twisted magnetic flux tubes can be obtained by increasing the magnetic field twist parameter, say taking, for instance, $\varepsilon = 0.4$. The dispersion curves and normalized wave growth rates of the kink ($m = \pm 1$)

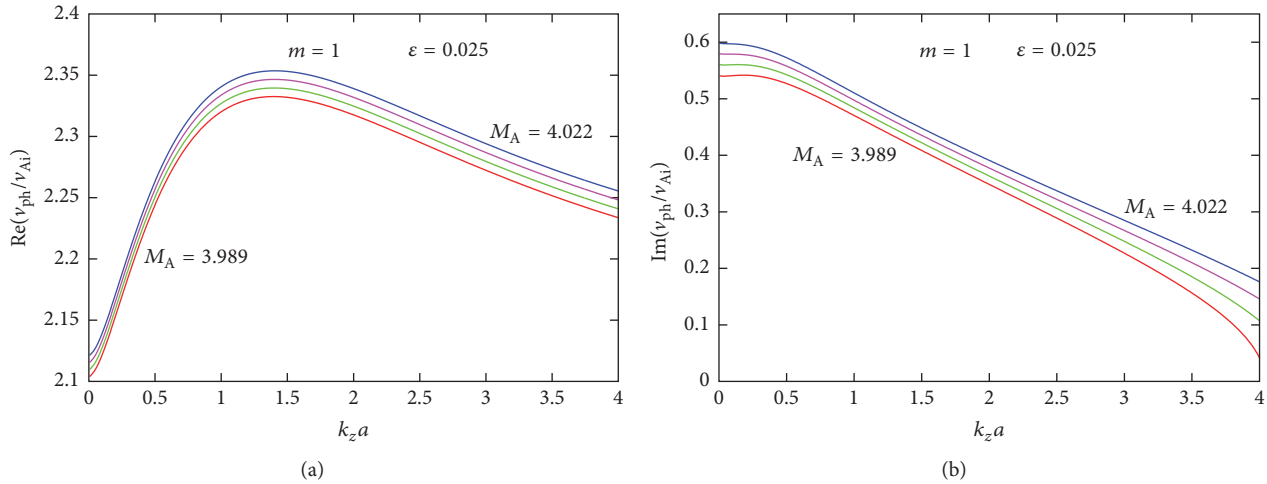

FIGURE 6: (a) Dispersion curves of unstable kink ($m = 1$) MHD mode propagating in a moving twisted flux tube of incompressible plasma (modeling jet #11) at $\eta = 0.896$ and $\varepsilon = 0.025$ and for $M_A = 3.989$, 4.0 (green curve), 4.011 (purple curve), and 4.022. (b) The normalized growth rates for the same values of M_A.

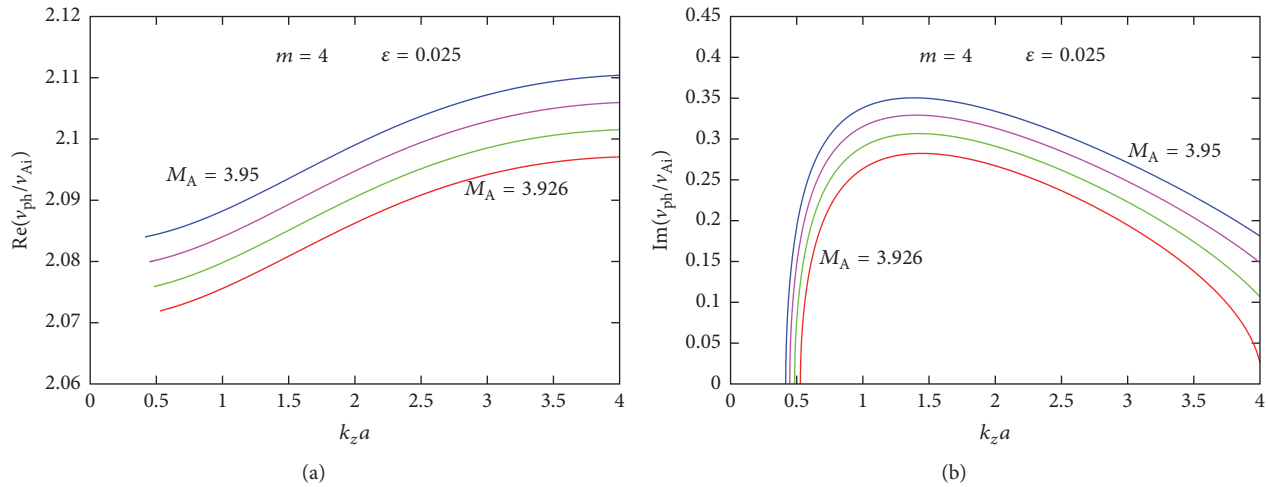

FIGURE 7: (a) Dispersion curves of unstable ($m = 4$) MHD mode propagating in a moving twisted flux tube of incompressible plasma at the same parameters as in Figure 6 for $M_A = 3.926$, 3.934 (green curve), 3.942 (purple curve), and 3.95. (b) The normalized growth rates for the same values of M_A.

mode are plotted in Figures 8 and 9. One is immediately seeing the rather complicated forms of both the dispersion curves and dimensionless growth rates of the $m = -1$ kink mode—such a complication was absent at $\varepsilon = 0.025$. We note that computations were performed at $b_{\text{twist}} = b/\sqrt{1+\varepsilon^2}$, and the reference "reduced" Alfvén speed inside the jet now is $v_{Ai}/\sqrt{1+\varepsilon^2} = 103\,\text{km s}^{-1}$. With this Alfvén speed the critical velocities for the instability occurrence are equal to $416\,\text{km s}^{-1}$ (for the $m = 1$ mode) and $\cong 408\,\text{km s}^{-1}$ for the $m = -1$ mode, respectively.

In solving dispersion equation (25) for the $m = 2$ MHD mode, we start with a little bit bigger Alfvén Mach number than that predicted by instability criterion (30) and have obtained three different kinds of dispersion curves and normalized growth rates (see Figure 10), notably curves with distinctive change of the normalized wave phase velocity in a relatively narrow $k_z a$-interval (the orange and blue curves in Figure 10(a)), two piece-wise dispersion curves (the purple and green curves in the same plot), and one almost linear dispersion curve (the red one which is in fact the marginal dispersion curve obtained for the threshold Alfvén Mach number equal to 4.062). Not less interesting are the dimensionless growth rate curves corresponding to these three kinds of dispersion curves. For the threshold Alfvén Mach number of 4.062 we obtained one instability window and instability starts at the critical dimensionless wave number of 1.944, or equivalently at $\lambda_{\text{cr}}^{m=2} \cong 8.0$ Mm. For the slightly superthreshold Alfvén Mach numbers of 4.075 and 4.1 we got two different instability windows (see the green and purple curves in Figure 10(b)) and a further increase in M_A leads to merging of those two instability windows—see the blue and orange curves in the same plot. The critical flow velocity at which KH instability arises is equal to $\cong 418\,\text{km s}^{-1}$.

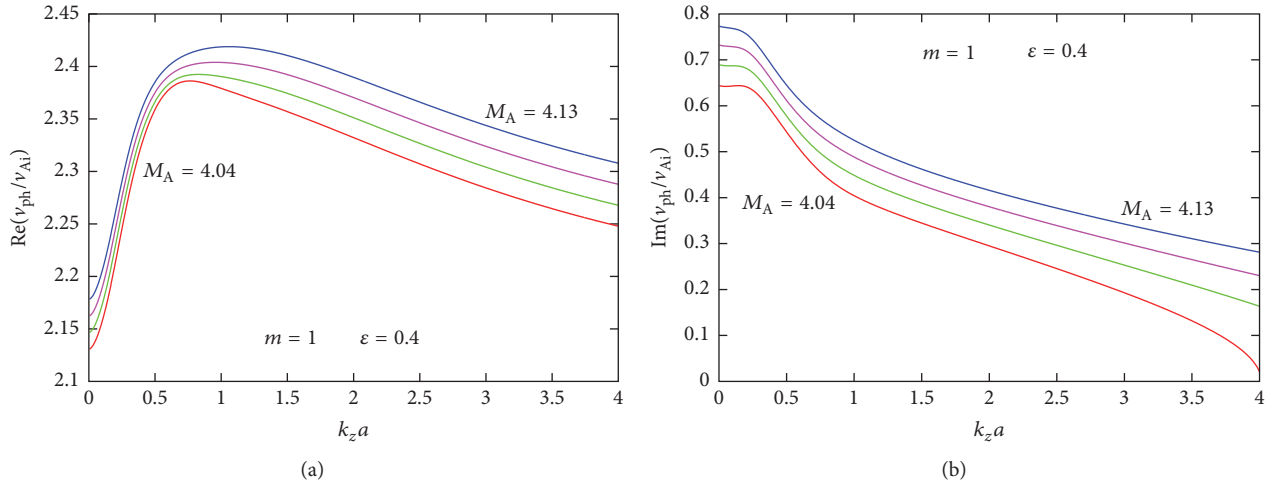

FIGURE 8: (a) Dispersion curves of unstable ($m = 1$) MHD mode propagating in a moving twisted flux tube of incompressible plasma (modeling jet #11) at $\eta = 0.896$ and $\varepsilon = 0.4$ and for $M_A = 4.04$, 4.07 (green curve), 4.1 (purple curve), and 4.13. (b) The normalized growth rates for the same values of M_A.

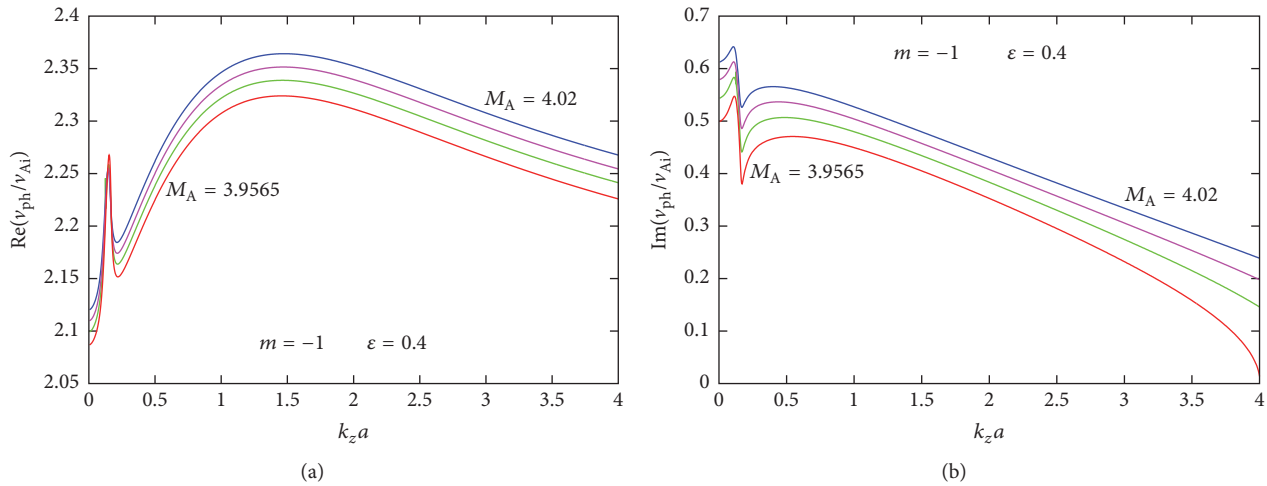

FIGURE 9: (a) Dispersion curves of unstable ($m = -1$) MHD mode propagating in a moving twisted flux tube of incompressible plasma (modeling jet #11) at the same parameters as in Figure 8 and for $M_A = 3.9565$, 3.98 (green curve), 4.0 (purple curve), and 4.02. (b) The normalized growth rates for the same values of M_A.

We have skipped the complicated dispersion and growth rate curves pictured in Figure 10 for the $m = 3$ and $m = 4$ MHD modes—we have calculated only a few curves for Alfvén Mach numbers close to the corresponding threshold ones (see Figures 11 and 12). One can observe that for the magnetic field twist parameter $\varepsilon = 0.4$ the critical dimensionless wave numbers are shifted far on the right—their values for both modes are equal to 3.619 and 4.512, respectively, that yield $\lambda_{cr}^{m=3} \cong 4.3$ Mm and $\lambda_{cr}^{m=4} \cong 3.5$ Mm. The critical jet speeds at which KH instability emerges are equal correspondingly to ≅422 and 424 km s^{-1}. We note that all the threshold Alfvén Mach numbers of higher MHD modes ($m \geqslant 2$) traveling on the moving twisted magnetic flux tube are larger than the predicted ones, but while for $\varepsilon = 0.025$ they (Alfvén Mach numbers) are decreasing with increasing the mode number, at $\varepsilon = 0.4$ we have just the opposite ordering. We would like to notice that finding the marginal dispersion and growth rate curves of the higher modes at $\varepsilon = 0.4$ turns out to be a laborious computational task.

To finish our survey on KH instability of MHD modes in moving twisted magnetic flux tubes, we will briefly consider how a weak twist of the internal magnetic field, $\varepsilon = 0.025$, will change the critical jet speeds for the occurrence of KH instability in jet #8. We are not going to graphically present the dispersion curves and growth rates of unstable modes because simply there is nothing special in their shape—in the incompressible plasma jet approximation and cool environment at small magnetic field twist the curves look, more or less, similar. Recall that at density contrast of 0.963 and magnetic fields ratio $b = 4.56$, the threshold Alfvén Mach number for the kink ($m = 1$) mode is equal to 6.9047,

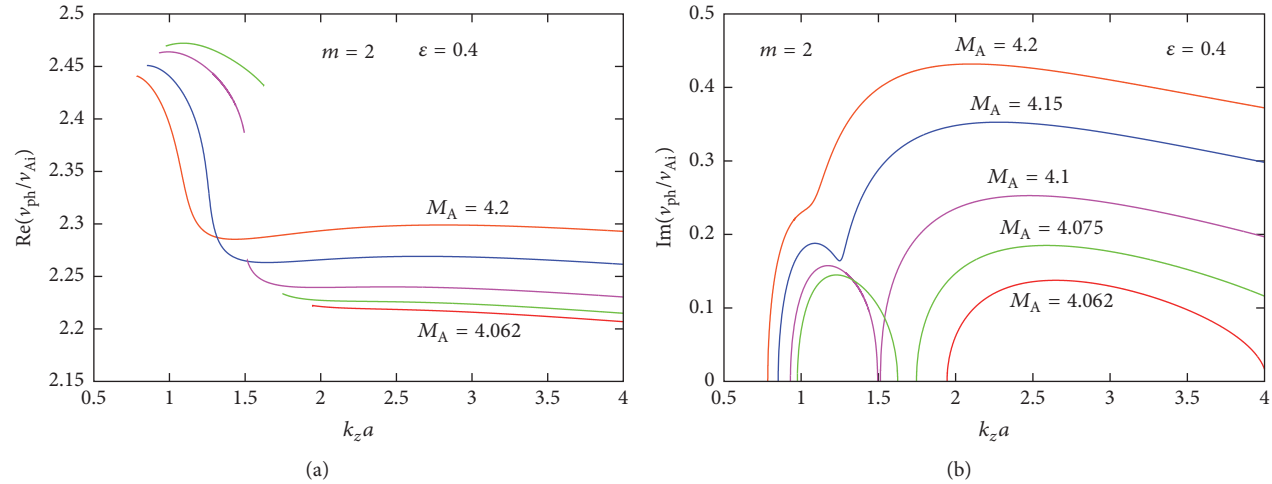

FIGURE 10: (a) Dispersion curves of unstable ($m = 2$) MHD mode propagating in a moving twisted flux tube of incompressible plasma (modeling jet #11) at the same parameters as in Figure 8 and for $M_A = 4.2, 4.15, 4.1, 4.075$, and 4.062. (b) The normalized growth rates for the same values of M_A.

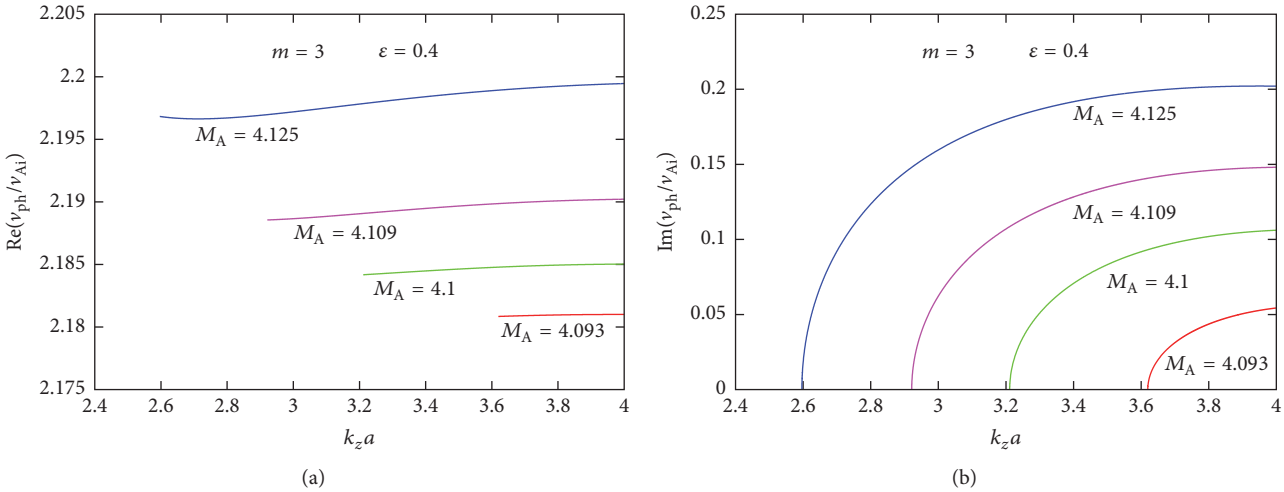

FIGURE 11: (a) Dispersion curves of unstable ($m = 3$) MHD mode propagating in a moving twisted flux tube of incompressible plasma (modeling jet #11) at the same parameters as in Figure 8 and for $M_A = 4.093, 4.1, 4.109$, and 4.125. (b) The normalized growth rates for the same values of M_A.

which for the reference Alfvén speed of 52.22 km s^{-1} yields a critical flow velocity of 360.6 km s^{-1} that is lower than the jet speed of 385 km s^{-1}. The KH instability of $m = 2$, 3, and 4 MHD modes should occur at flow velocities of ≅259, 357, and 355.5 km s^{-1} and start at critical dimensionless wave numbers $(k_z a)_{cr}$ equal, respectively, to 0.054, 0.119, and 0.205.

4. Summary and Conclusion

In this paper, we have explored the conditions under which MHD waves with various mode numbers ($m = \pm 1$, 2, 3, and 4) propagating along untwisted and twisted magnetic flux tubes (representing three observed X-ray solar jets) can become unstable against the KH instability. We have used two models of a soft X-ray jet, namely, considering the jet and its surrounding coronal medium as compressible magnetized plasmas and another simplified model representing the jet as an incompressible medium and its environment as cool coronal plasma. A comparison of the dispersion curves and normalized wave growth rates of the kink ($m = 1$) mode calculated on the base of these two models shows that one obtains similar dispersion curves' and growth rates' patterns (see Figures 2 and 3). This circumstance justifies the usage of the second, simplified, model in studying the propagation characteristics of MHD modes in moving twisted magnetic flux tubes. We must, however, immediately underline that the onset of KH instability in incompressible magnetic flux tube always requires slightly greater threshold Alfvén Mach numbers and correspondingly higher critical jet speeds.

Our numerical computations show the following:

(i) The flow does not change the nature of propagating stable MHD modes being pure surface waves in a

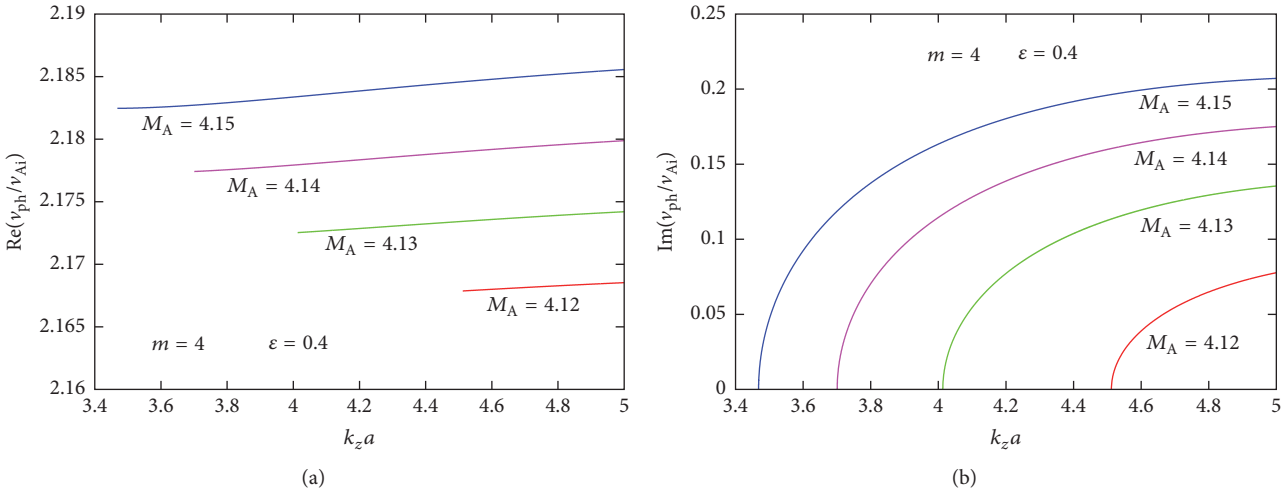

FIGURE 12: (a) Dispersion curves of unstable ($m = 4$) MHD mode propagating in a moving twisted flux tube of incompressible plasma (modeling jet #11) at the same parameters as in Figure 8 and for $M_A = 4.12$, 4.13, 4.14, and 4.15. (b) The normalized growth rates for the same values of M_A.

rest magnetic flux tube, but unstable ones due to high enough jet speed become partly surface and partly leaky waves. That is why it is more appropriate to term them *generalized surface waves*.

(ii) The KH instability of the kink mode ($m = \pm 1$) starts at Alfvén Mach numbers very close to the predicted ones. Numerically found threshold M_As for the higher MHD modes are, in fact, greater than their initial evaluations. Accessible flow velocities for instability onset in jet #11 have been derived for moving untwisted magnetic flux tube of compressible plasma (429 km s^{-1}) and for the $m = 4$ MHD mode propagating in weakly twisted magnetic flux tube ($\varepsilon = 0.025$) of incompressible plasma surrounded by cool coronal medium (435.6 km s^{-1}). A nonnegligible decrease of the critical jet speed for all considered modes running in twisted moving flux tube is obtained when the magnetic field twist parameter is $\varepsilon = 0.4$—then the critical velocities of the $m = \pm 1$, 2, 3, and 4 modes are equal to 416, ≅408, 418, ≅422, and 424 km s^{-1}, respectively. The instability onset of all considered MHD modes in jet #8 occurs at flow velocities, in general, lower than the jet speed of 385 km s^{-1}—their magnitudes for the kink ($m = 1$) mode running on untwisted or slightly twisted magnetic flux tube (with magnetic field twist parameter $\varepsilon = 0.025$) are equal to 348.3 and 360.6 km s^{-1}, respectively. The corresponding critical flow velocities for the higher ($m = 2$, 3, and 4) MHD modes turn out to lie between aforementioned speeds, namely, being equal to ≅359, 35,7 and 355.5 km s^{-1}. Jet #16 possessing the highest flow speed of 532 km s^{-1} in Shimojo and Shibata's Events List [10] is, however, stable against the KH instability—the critical flow velocity at which the kink ($m = 1$) mode would become unstable propagating in untwisted magnetic flux tube is equal to ≅826 km s^{-1}—much higher than the jet speed. The critical velocities in twisted tubes are even larger, equal to 852.4, 848.3, 844.8, and 842.6 km s^{-1} for the m = 1–4 MHD modes, respectively.

(iii) The instability onset for a given mode m is very sensitive to the main input parameters: density contrast, η, magnetic field ratio, b, the magnetic field twist ε, and especially the background magnetic field B_e. If we assume that, for jet #11 $B_e = 10$ G, Alfvén speeds in the two media have new values, notably $v_{Ai} = 320.38$ km s^{-1} and $v_{Ae} = 427.5$ km s^{-1}. With these new Alfvén speeds the input parameters for solving wave dispersion relations (9) and (25) have changed and more specifically $\widetilde{\beta}_i = 0.7376$, $\widetilde{\beta}_e = 0.1506$, and $b = 1.2636$. Now the critical jet velocity for the instability onset dramatically increases—it becomes 751 km s^{-1} for the kink mode in untwisted tube and 774 km s^{-1} in weakly twisted ($\varepsilon = 0.025$) flux tube.

(iv) If we accept the Paraschiv's et al. [90] suggestion that plasma density in the region crossed by coronal jets has to be the sum $n_{cor} + n_{jet}$ or, on average, two times higher than the plasma in the surrounding corona n_{cor}; then the total pressure balance equation, again for jet #11, can be satisfied at $B_e = 10$ G and we have the following set of input parameters: $\eta = 0.437$, $v_{Ai} = 105.7$ km s^{-1}, $v_{Ae} = 427.5$ km s^{-1}, $\widetilde{\beta}_i = 6.7782$, $\widetilde{\beta}_e = 0.1506$, and $b = 3.781$. With these parameters the critical flow velocities for KH instability occurrence reduce to 560 km s^{-1} for the kink mode in untwisted flux tube and to 575 km s^{-1} for the same mode in weakly twisted ($\varepsilon = 0.025$) flux tube. Note that within this approach one obtains critical jet speeds that are approximately with 200 km s^{-1} less than those calculated for the same background magnetic field of 10 G. Here one raises the big question: "which

approach, the standard one or that of Paraschiv's et al. [90], will be appropriate for studying/modeling the KH instability in solar X-ray (and other) jets?" The perfect answer to this question will be obtained when we will try to model a really observationally detected KH instability in soft X-ray jets like that of Foullon et al. [57].

It is intriguing to see what critical jet speeds we will obtain for a numerically modeled solar X-jet—a case in point is the study of Miyagoshi and Yokoyama [91]. These authors have presented MHD numerical simulations of solar X-ray jets based on magnetic reconnection model that includes chromospheric evaporation. Peculiar to their study is that total pressure balance equation excludes the magnetic pressure inside the jet saying that it is very weak; that is (in their notation),

$$p_{\text{jet}} = p_{\text{cor}} + \frac{B^2}{2\mu}, \tag{32}$$

where $B \equiv B_{\text{e}}$ is the background (coronal) magnetic field. Supposing that $n_{\text{cor}} = 10^9\,\text{cm}^{-3}$, $T_{\text{cor}} = 10^6\,\text{K}$, $B = 10\,\text{G}$, and $n_{\text{jet}} = 4.5 \times 10^9\,\text{cm}^{-3}$, they obtain from their total balance equation the temperature of the jet, $T_{\text{jet}} = 6.7 \times 10^6\,\text{K}$—indeed a reasonable value. However, to satisfy the standard total pressure balance (1) (assuming a very small, but finite value for the magnetic field in the jet, B_{i}), with the aforementioned values for both the temperature and jet density, we were forced to double the coronal density, that is, to take $n_{\text{cor}} \equiv n_{\text{e}} = 2.0 \times 10^9\,\text{cm}^{-3}$. In such a case the sound and Alfvén speeds in the jet and its environment are $c_{\text{si}} \cong 304\,\text{km s}^{-1}$, $c_{\text{se}} = 117\,\text{km s}^{-1}$, $v_{\text{Ai}} = 47.67\,\text{km s}^{-1}$, and $v_{\text{Ae}} = 487.5\,\text{km s}^{-1}$. The ordering of sound and Alfvén speeds is the same as for the #11 X-ray jet in the Shimojo and Shibata paper [10] that implies the propagation of pure surface stable modes. The magnetic field inside the jet is $B_{\text{i}} \cong 1.47\,\text{G}$—hence the magnetic fields ratio is $b = 6.817$. Thus the input parameters for solving (9) and (25) are $\eta = 0.444$, $\widetilde{\beta}_{\text{i}} = 40.5872$, and $\widetilde{\beta}_{\text{e}} = 0.0695$ and, as we already found, $b = 6.817$. Note that this relatively high value of b would suspect a rather big value of the threshold Alfvén Mach number—the instability criterion yields $M_{\text{A}} > 12.42$. Numerically found threshold M_{A} for initiating KH instability of the kink ($m = 1$) mode in moving untwisted magnetic flux tube of compressible plasma is 12.435 that yields a critical velocity of $607\,\text{km s}^{-1}$. For the case of weakly twisted flux tube ($\varepsilon = 0.025$) in the approximation incompressible jet and cool plasma environment we obtained for the same kink mode a critical velocity of $620\,\text{km s}^{-1}$. The critical speeds for the higher ($m = 2$–4) modes are accordingly of 615, 609, and $606\,\text{km s}^{-1}$.

The three examples of coronal X-jets embedded in a background magnetic field of 10 G show that KH instability of basically the kink ($m = 1$) mode can occur if jets' speeds lie in the range of 500–700 km s^{-1}. Such velocities are generally accessible for high-speed jets; lower critical speeds between 400 and $500\,\text{km s}^{-1}$ can be observed/detected at moderate external magnetic fields in the range of 6–7 G. This requirement is in agreement with Pucci et al. [34] evaluation that the magnetic field inside a standard X-ray jet would be equal to 2.8 G, while for a blowout jet that value should be around 4.5 G. To be honest, we can say that the most of soft X-ray solar jets with speeds below 400–450 km s^{-1} are stable against the KH instability—this instability can develop only in relatively dense high-speed jets. Note, however, that each soft X-ray jet is a unique event—it requires a separate careful exploration of the instability conditions. Arising KH instability in turn might trigger wave turbulence considered as an effective mechanism for coronal heating.

Our simplified model of studying the possibilities for emerging of KH instability in fast soft X-ray jets has to be improved by assuming a radial density gradient or some magnetic field and flow velocity shears. A challenge also is the modeling of the same instability in rotating and oscillatory swaying coronal hole X-ray jets.

Competing Interests

The authors declare that they have no competing interests.

Acknowledgments

This work was supported by the Bulgarian Science Fund and the Department of Science & Technology, Government of India Fund, under Indo-Bulgarian Bilateral Project DNTS/INDIA 01/7, /Int/Bulgaria/P-2/12. The authors are indebted to Snezhana Yordanova for drawing one figure.

References

[1] J. M. Beckers, "Solar spicules," *Annual Review of Astronomy and Astrophysics*, vol. 10, no. 1, pp. 73–100, 1972.

[2] J. R. Roy, "The magnetic properties of solar surges," *Solar Physics*, vol. 28, no. 1, pp. 95–114, 1973.

[3] K. Shibata, T. Nakamura, T. Matsumoto et al., "Chromospheric anemone jets as evidence of ubiquitous reconnection," *Science*, vol. 318, no. 5856, pp. 1591–1594, 2007.

[4] C. Chifor, H. Isobe, E. Mason et al., "Magnetic flux cancellation associated with a recurring solar jet observed with Hinode, RHESSI, and STEREO/EUVI," *Astronomy & Astrophysics*, vol. 491, no. 1, pp. 279–288, 2008.

[5] N. Nishizuka, M. Shimizu, T. Nakamura et al., "Giant chromospheric anemone jet observed with *Hinode* and comparison with magnetohydrodynamic simulations: Evidence of propagating Alfvén waves and magnetic reconnection," *The Astrophysical Journal Letters*, vol. 683, no. 1, pp. L83–L86, 2008.

[6] D. Alexander and L. Fletcher, "High-resolution observations of plasma jets in the solar corona," *Solar Physics*, vol. 190, no. 1-2, pp. 167–184, 1999.

[7] K. Shibata, Y. Ishido, L. Acton et al., "Observations of X-ray jets with the Yohkoh soft X-ray telescope," *Publications of the Astronomical Society of Japan*, vol. 44, no. 5, pp. L173–L179, 1992.

[8] S. Tsuneta, L. Acton, M. Bruner et al., "The soft X-ray telescope for the SOLAR-A mission," *Solar Physics*, vol. 136, no. 1, pp. 37–67, 1991.

[9] M. Shimojo, S. Hashimoto, K. Shibata, T. Hirayama, H. S. Hudson, and L. W. Acton, "Statistical study of solar X-ray jets observed with the Yohkoh soft X-ray telescope," *Publications of*

the Astronomical Society of Japan, vol. 48, no. 1, pp. 123–136, 1996.

[10] M. Shimojo and K. Shibata, "Physical parameters of solar X-ray jets," *The Astrophysical Journal*, vol. 542, no. 2, pp. 1100–1108, 2000.

[11] L. Culhane, L. K. Harra, D. Baker et al., "Hinode EUV study of jets in the Sun's south polar corona," *Publications of the Astronomical Society of Japan*, vol. 59, supplement 3, pp. S751–S756, 2007.

[12] C. Chifor, P. R. Young, H. Isobe et al., "An active region jet observed with Hinode," *Astronomy & Astrophysics*, vol. 481, no. 1, pp. L57–L60, 2008.

[13] A. Savcheva, J. Cirtain, E. E. DeLuca et al., "A study of polar jet parameters based on Hinode XRT observations," *Publications of the Astronomical Society of Japan*, vol. 59, supplement 3, pp. S771–S778, 2007.

[14] J. W. Cirtain, L. Golub, L. Lundquist et al., "Evidence for Alfvén waves in solar X-ray jets," *Science*, vol. 318, no. 5856, pp. 1580–1582, 2007.

[15] Y.-H. Kim, Y.-J. Moon, Y.-D. Park et al., "Small-scale X-ray/EUV jets seen in Hinode XRT and TRACE," *Publications of the Astronomical Society of Japan*, vol. 59, supplement 3, pp. S763–S769, 2007.

[16] L.-H. Yang, Y.-C. Jiang, J.-Y. Yang, Y. Bi, R.-S. Zheng, and J.-C. Hong, "Observations of EUV and soft X-ray recurring jets in an active region," *Research in Astronomy and Astrophysics*, vol. 11, no. 10, pp. 1229–1242, 2011.

[17] M. S. Madjarska, "Dynamics and plasma properties of an X-ray jet from SUMER, EIS, XRT, and EUVI A & B simultaneous observations," *Astronomy & Astrophysics*, vol. 526, no. 2, article A19, 2011.

[18] K. Chandrashekhar, A. Bemporad, D. Banerjee, G. R. Gupta, and L. Teriaca, "Characteristics of polar coronal hole jets," *Astronomy & Astrophysics*, vol. 561, article A104, 2014.

[19] W. D. Pesnell, B. J. Thompson, and P. C. Chamberlin, "The *Solar Dynamics Observatory* (SDO)," *Solar Physics*, vol. 275, no. 1, pp. 3–15, 2012.

[20] J. R. Lemen, A. M. Title, D. J. Akin et al., "The *Atmospheric Imaging Assembly* (AIA) on the *Solar Dynamics Observatory* (SDO)," *Solar Physics*, vol. 275, no. 1, pp. 17–40, 2012.

[21] P. Boerner, C. Edwards, J. Lemen et al., "Initial calibration of the *Atmospheric Imaging Assembly* (AIA) on the *Solar Dynamics Observatory* (SDO)," *Solar Physics*, vol. 275, no. 1, pp. 41–66, 2012.

[22] S. P. Moschou, K. Tsinganos, A. Vourlidas, and V. Archontis, "SDO observations of solar jets," *Solar Physics*, vol. 284, no. 2, pp. 427–438, 2013.

[23] K. Chandrashekhar, R. J. Morton, D. Banerjee, and G. R. Gupta, "The dynamical behaviour of a jet in an on-disk coronal hole observed with AIA/SDO," *Astronomy & Astrophysics*, vol. 562, article A98, 2014.

[24] A. C. Sterling, R. L. Moore, D. A. Falconer, and M. Adams, "Small-scale filament eruptions as the driver of X-ray jets in solar coronal holes," *Nature*, vol. 523, no. 7561, pp. 437–440, 2015.

[25] B. Filippov, A. K. Srivastava, B. N. Dwivedi et al., "Formation of a rotating jet during the filament eruption on 2013 April 10-11," *Monthly Notices of the Royal Astronomical Society*, vol. 451, no. 1, pp. 1117–1129, 2015.

[26] M. Shimojo, K. Shibata, T. Yokoyama, and K. Hori, "One-dimensional and pseudo-two-dimensional hydrodynamic simulations of solar X-ray jets," *Astrophysical Journal*, vol. 550, no. 2, pp. 1051–1063, 2001.

[27] S. Kamio, H. Hara, T. Watanabe et al., "Velocity structure of jets in a coronal hole," *Publications of the Astronomical Society of Japan*, vol. 59, supplement 3, pp. S757–S762, 2007.

[28] R. L. Moore, J. W. Cirtain, A. C. Sterling, and D. A. Falconer, "Dichotomy of solar coronal jets: Standard jets and blowout jets," *The Astrophysical Journal*, vol. 720, no. 1, pp. 757–770, 2010.

[29] E. Pariat, S. K. Antiochos, and C. R. DeVore, "A model for solar polar jets," *The Astrophysical Journal*, vol. 691, no. 1, pp. 61–74, 2009.

[30] B. Filippov, L. Golub, and S. Koutchmy, "X-ray jet dynamics in a polar coronal hole region," *Solar Physics*, vol. 254, no. 2, pp. 259–269, 2009.

[31] E. Pariat, S. K. Antiochos, and C. R. Devore, "Three-dimensional modeling of quasi-homologous solar jets," *Astrophysical Journal*, vol. 714, no. 2, pp. 1762–1778, 2010.

[32] F. Jiang, J. Zhang, and S. Yang, "Interaction between an emerging flux region and a pre-existing fan-spine dome observed by IRIS and SDO," *Publications of the Astronomical Society of Japan*, vol. 67, no. 4, article 78, 2015.

[33] A. C. Sterling, L. K. Harra, and R. L. Moore, "Fibrillar chromospheric spicule-like counterparts to an extreme-ultraviolet and soft X-ray blowout coronal jet," *The Astrophysical Journal*, vol. 722, no. 2, pp. 1644–1653, 2010.

[34] S. Pucci, G. Poletto, A. C. Sterling, and M. Romoli, "Physical parameters of standard and blowout jets," *Astrophysical Journal*, vol. 776, article 16, 2013.

[35] R. L. Moore, A. C. Sterling, D. A. Falconer, and D. Robe, "The cool component and the dichotomy, lateral expansion, and axial rotation of solar X-ray jets," *The Astrophysical Journal*, vol. 769, no. 2, article 134, 2013.

[36] R. L. Moore, A. C. Sterling, and D. A. Falconer, "Magnetic untwisting in solar jets that go into the outer corona in polar coronal holes," *Astrophysical Journal*, vol. 806, no. 1, article 11, 2015.

[37] G. E. Brueckner, R. A. Howard, M. J. Koomen et al., "The Large Angle Spectroscopic Coronagraph (LASCO)," *Solar Physics*, vol. 162, no. 1, pp. 357–402, 1995.

[38] B. Schmieder, Y. Guo, F. Moreno-Insertis et al., "Twisting solar coronal jet launched at the boundary of an active region," *Astronomy and Astrophysics*, vol. 559, article A1, 2013.

[39] E. Pariat, K. Dalmasse, C. R. DeVore, S. K. Antiochos, and J. T. Karpen, "Model for straight and helical solar jets: I. Parametric studies of the magnetic field geometry," *Astronomy and Astrophysics*, vol. 573, article 130, 2015.

[40] S. Patsourakos, E. Pariat, A. Vourlidas, S. K. Antiochos, and J. P. Wuelser, "*STEREO* SECCHI stereoscopic observations constraining the initiation of polar coronal jets," *The Astrophysical Journal*, vol. 680, no. 1, pp. L73–L76, 2008.

[41] C. Gontikakis, V. Archontis, and K. Tsinganos, "Observations and 3D MHD simulations of a solar active region jet," *Astronomy & Astrophysics*, vol. 506, no. 3, pp. L45–L48, 2009.

[42] R. Chandra, G. R. Gupta, S. Mulay, and D. Tripathi, "Sunspot waves and triggering of homologous active region jets," *Monthly Notices of the Royal Astronomical Society*, vol. 446, no. 4, pp. 3741–3748, 2015.

[43] J. Chae, H. Wang, C.-Y. Lee, P. R. Goode, and U. Schühle, "Photospheric magnetic field changes associated with transition

region explosive events," *Astrophysical Journal*, vol. 497, no. 2, pp. L109–L112, 1998.

[44] L. R. B. Rubio and C. Beck, "Magnetic flux cancellation in the moat of sunspots: results from simultaneous vector spectropolarimetry in the visible and the infrared," *Astrophysical Journal*, vol. 626, no. 2, pp. L125–L128, 2005.

[45] L. Heggland, B. De Pontieu, and V. H. Hansteen, "Observational signatures of simulated reconnection events in the solar chromosphere and transition region," *The Astrophysical Journal*, vol. 702, no. 1, pp. 1–18, 2009.

[46] D. E. Innes, R. H. Cameron, and S. K. Solanki, "EUV jets, type III radio bursts and sunspot waves investigated using SDO/AIA observations," *Astronomy and Astrophysics*, vol. 531, article L13, 2011.

[47] A. K. Srivastava and K. Murawski, "Observations of a pulse-driven cool polar jet by SDO/AIA," *Astronomy & Astrophysics*, vol. 534, article A62, 2011.

[48] S. Chandrasekhar, *Hydrodynamic and Hydromagnetic Stability*, The International Series of Monographs on Physics, Clarendon Press, Oxford, UK, 1961.

[49] T. V. Zaqarashvili, I. Zhelyazkov, and L. Ofman, "Stability of rotating magnetized jets in the solar atmosphere. I. Kelvin–Helmholtz instability," *Astrophysical Journal*, vol. 813, no. 2, article 123, 2015.

[50] D. Ryu, T. W. Jones, and A. Frank, "The magnetohydrodynamic Kelvin-Helmholtz instability: A three-dimensional study of nonlinear evolution," *The Astrophysical Journal*, vol. 545, no. 1, pp. 475–493, 2000.

[51] S. A. Maslowe, "Shear flow instabilities and transition," in *Hydromagnetic Instabilities and the Transition to Turbulence*, H. L. Swinney and J. P. Gollub, Eds., pp. 181–228, Springer, Berlin, Germany, 1985.

[52] T. E. Berger, G. Slater, N. Hurlburt et al., "Quiescent prominence dynamics observed with the Hinode solar optical telescope. I. Turbulent upflow plumes," *The Astrophysical Journal*, vol. 716, no. 2, pp. 1288–1307, 2010.

[53] M. Ryutova, T. Berger, Z. Frank, T. Tarbell, and A. Title, "Observation of plasma instabilities in quiescent prominences," *Solar Physics*, vol. 267, no. 1, pp. 75–94, 2010.

[54] D. Martínez-Gómez, R. Soler, and J. Terradas, "Onset of the Kelvin-Helmholtz instability in partially ionized magnetic flux tubes," *Astronomy and Astrophysics*, vol. 578, article A104, 2015.

[55] N. F. Loureiro, A. A. Schekochihin, and D. A. Uzdensky, "Plasmoid and Kelvin-Helmholtz instabilities in Sweet-Parker current sheets," *Physical Review E: Statistical, Nonlinear, and Soft Matter Physics*, vol. 87, no. 1, article 013102, 2013.

[56] L. Feng, B. Inhester, and W. Q. Gan, "Kelvin–Helmholtz instability of a coronal streamer," *Astrophysical Journal*, vol. 774, no. 2, article 141, 2013.

[57] C. Foullon, E. Verwichte, V. M. Nakariakov, K. Nykyri, and C. J. Farrugia, "Magnetic Kelvin–Helmholtz instability at the Sun," *Astrophysical Journal Letters*, vol. 729, no. 1, article L8, 2011.

[58] L. Ofman and B. J. Thompson, "*SDO*/AIA observation of Kelvin–Helmholtz instability in the solar corona," *The Astrophysical Journal Letters*, vol. 734, no. 1, article L11, 2011.

[59] C. Foullon, E. Verwichte, K. Nykyri, M. J. Aschwanden, and I. G. Hannah, "Kelvin–Helmholtz instability of the CME reconnection outflow layer in the low corona," *The Astrophysical Journal*, vol. 767, no. 2, article 170, 2013.

[60] U. V. Möstl, M. Temmer, and A. M. Veronig, "The Kelvin–Helmholtz instability at coronal mass ejection boundaries in the solar corona: Observations and 2.5D MHD simulations," *Astrophysical Journal Letters*, vol. 766, no. 1, article 12, 2013.

[61] K. Nykyri and C. Foullon, "First magnetic seismology of the CME reconnection outflow layer in the low corona with 2.5-D MHD simulations of the Kelvin-Helmholtz instability," *Geophysical Research Letters*, vol. 40, no. 16, pp. 4154–4159, 2013.

[62] T. V. Zaqarashvili, A. J. Díaz, R. Oliver, and J. L. Ballester, "Instability of twisted magnetic tubes with axial mass flows," *Astronomy & Astrophysics*, vol. 516, article A84, 2010.

[63] R. Soler, A. J. Díaz, J. L. Ballester, and M. Goossens, "Kelvin–Helmholtz instability in partially ionized compressible plasmas," *The Astrophysical Journal*, vol. 749, no. 2, article 163, 2012.

[64] T. V. Zaqarashvili, "Solar spicules: recent challenges in observations and theory," in *Proceedings of the 3rd School and Workshop on Space Plasma Physics*, I. Zhelyazkov and T. Mishonov, Eds., vol. 1356 of *AIP Conference Proceedings*, pp. 106–116, AIP Publishing LLC, Melville, NY, USA, 2011.

[65] I. Zhelyazkov, "Magnetohydrodynamic waves and their stability status in solar spicules," *Astronomy & Astrophysics*, vol. 537, article A124, 2012.

[66] A. Ajabshirizadeh, H. Ebadi, R. E. Vekalati, and K. Molaverdikhani, "The possibility of Kelvin-Helmholtz instability in solar spicules," *Astrophysics and Space Science*, vol. 357, no. 1, article 33, 2015.

[67] I. Zhelyazkov and T. V. Zaqarashvili, "Kelvin-Helmholtz instability of kink waves in photospheric twisted flux tubes," *Astronomy & Astrophysics*, vol. 547, article A14, 2012.

[68] I. Zhelyazkov, R. Chandra, A. K. Srivastava, and T. Mishonov, "Kelvin–Helmholtz instability of magnetohydrodynamic waves propagating on solar surges," *Astrophysics and Space Science*, vol. 356, no. 2, pp. 231–240, 2015.

[69] I. Zhelyazkov, T. V. Zaqarashvili, R. Chandra, A. K. Srivastava, and T. Mishonov, "Kelvin–Helmholtz instability in solar cool surges," *Advances in Space Research*, vol. 56, no. 12, pp. 2727–2737, 2015.

[70] I. Zhelyazkov, R. Chandra, and A. K. Srivastava, "Can magnetohydrodynamic waves traveling on solar dark mottles become unstable?" *Bulgarian Journal of Physics*, vol. 42, no. 1, pp. 68–87, 2015.

[71] I. Zhelyazkov, T. V. Zaqarashvili, and R. Chandra, "Kelvin-Helmholtz instability in coronal mass ejecta in the lower corona," *Astronomy and Astrophysics*, vol. 574, 2015.

[72] I. Zhelyazkov, R. Chandra, and A. K. Srivastava, "Kelvin–Helmholtz instability in coronal mass ejections and solar surges," in *Proceedings of the 5th School and Workshop on Space Plasma Physics*, I. Zhelyazkov and T. Mishonov, Eds., vol. 1714 of *AIP Conference Proceedings*, AIP Publishing LLC, Melville, NY, USA, article 030005, 2016.

[73] D. Kuridze, V. Henriques, M. Mathioudakis et al., "The dynamics of rapid redshifted and blueshifted excursions in the solar Hα line," *The Astrophysical Journal*, vol. 802, no. 1, article 26, 2015.

[74] I. Zhelyazkov, "On modeling the Kelvin–Helmholtz instability in solar atmosphere," *Journal of Astrophysics and Astronomy*, vol. 36, no. 1, pp. 233–254, 2015.

[75] S. Vasheghani Farahani, T. Van Doorsselaere, E. Verwichte, and V. M. Nakariakov, "Propagating transverse waves in soft X-ray coronal jets," *Astronomy & Astrophysics*, vol. 498, no. 2, pp. L29–L32, 2009.

[76] I. Zhelyazkov, "Review of the magnetohydrodynamic waves and their stability in solar spicules and X-ray jets," in *Topics in Magnethydrodynamics*, L. Zheng, Ed., chapter 6, InTech, Rijeka, Croatia, 2012.

[77] I. Zhelyazkov, "Kelvin–Helmholtz instability of kink waves in photospheric, chromospheric, and X-ray solar jets," in *Proceedings of the 4th School and Workshop on Space Plasma Physics*, I. Zhelyazkov and T. Mishonov, Eds., vol. 1551, pp. 150–164, AIP Publishing LLC, Melville, NY, USA, 2013.

[78] M. Goossens, J. V. Hollweg, and T. Sakurai, "Resonant behaviour of MHD waves on magnetic flux tubes. III. Effect of equilibrium flow," *Solar Physics*, vol. 138, no. 2, pp. 233–255, 1992.

[79] K. Hain and R. Lüst, "Zur Stabilität zylindersymmetrischer Plasmakonfigurationen mit Volumenströmen," *Zeitschrift für Naturforschung*, vol. 13, pp. 936–940, 1958.

[80] J. P. Goedbloed, "Stabilization of magnetohydrodynamic instabilities by force-free magnetic fields: I. Plane plasma layer," *Physica*, vol. 53, no. 3, pp. 412–444, 1971.

[81] T. Sakurai, M. Goossens, and J. V. Hollweg, "Resonant behaviour of MHD waves on magnetic flux tubes. I. Connection formulae at the resonant surfaces," *Solar Physics*, vol. 133, no. 2, pp. 227–245, 1991.

[82] P. M. Edwin and B. Roberts, "Wave propagation in a magnetic cylinder," *Solar Physics*, vol. 88, no. 1-2, pp. 179–191, 1983.

[83] M. Terra-Homem, R. Erdélyi, and I. Ballai, "Linear and nonlinear MHD wave propagation in steady-state magnetic cylinders," *Solar Physics*, vol. 217, no. 2, pp. 199–223, 2003.

[84] V. M. Nakariakov, "MHD oscillations in solar and stellar coronae: current results and perspectives," *Advances in Space Research*, vol. 39, no. 12, pp. 1804–1813, 2007.

[85] K. Bennett, B. Roberts, and U. Narain, "Waves in twisted magnetic flux tubes," *Solar Physics*, vol. 185, no. 1, pp. 41–59, 1999.

[86] P. S. Cally, "Leaky and non-leaky oscillations in magnetic flux tubes," *Solar Physics*, vol. 103, no. 2, pp. 277–298, 1986.

[87] I. Zhelyazkov, R. Chandra, and A. K. Srivastava, "Kelvin-Helmholtz instability in an active region jet observed with Hinode," *Astrophysics and Space Science*, vol. 361, no. 2, article 51, 2016.

[88] T. V. Zaqarashvili, Z. Vörös, and I. Zhelyazkov, "Kelvin-Helmholtz instability of twisted magnetic flux tubes in the solar wind," *Astronomy & Astrophysics*, vol. 561, article A62, 2014.

[89] J. W. Dungey and R. E. Loughhead, "Twisted magnetic fields in conducting fluids," *Australian Journal of Physics*, vol. 7, no. 1, pp. 5–13, 1954.

[90] A. R. Paraschiv, A. Bemporad, and A. C. Sterling, "Physical properties of solar polar jets: A statistical study with Hinode XRT data," *Astronomy & Astrophysics*, vol. 579, article A96, 2015.

[91] T. Miyagoshi and T. Yokoyama, "Magnetohydrodynamic numerical simulations of solar X-ray jets based on the magnetic reconnection model that includes chromospheric evaporation," *The Astrophysical Journal*, vol. 593, no. 2, pp. L133–L136, 2003.